Macromolecules

ARTICLE

pubs.acs.org/Macromolecules

Dynamics of Polyisoprene-Poly(*p-tert*-butylstyrene) Diblock Copolymer in Disordered State

Quan Chen, Yumi Matsumiya, Yuichi Masubuchi, and Hiroshi Watanabe*

Institute for Chemical Research, Kyoto University, Uji, Kyoto 611-0011, Japan

Tadashi Inoue

Department of Macromolecular Science, Faculty of Science, Osaka University, Toyonaka, Osaka 560-0043, Japan

ABSTRACT: Linear viscoelastic and dielectric behavior was examined for a diblock copolymer composed of *cis*-polyisoprene (PI) and poly(*p-tert*-butylstyrene) (PtBS) blocks of the molecular weights $M_{PI} = 52.6 \times 10^3$ and $M_{PtBS} = 41.8 \times 10^3$ (PI weight fraction $w_{PI} = 55.7$ wt %). These blocks were miscible and the copolymer was in the disordered state at temperatures examined, $20 \leq T/°C \leq 120$. PI has the type-A dipole parallel along the chain backbone while PtBS does not. Thus, the dielectric response at low frequencies exclusively detected the global motion (end-to-end vector fluctuation) of the PI block, while the viscoelastic response reflected the motion of the copolymer chain as a whole. The dielectric data of the PI block exhibited prominent thermo-rheological complexity. Since the PI and PtBS blocks behaved as the fast and slow blocks at low T and this difference of their relaxation rates decreased at high T, the complexity was related partly to the dynamic frictional heterogeneity for the PI block resulting from this dynamic asymmetry of the two blocks. However, it turned out that the complexity was more importantly related to the connectivity between the PI and PtBS blocks: Namely, the PI block possibly behaved as a tethered chains at low T (where the slow PtBS block effectively anchored the PI block) and as a portion of a free linear chain at high T (where this anchoring effect vanished), and this change in the motional mode of the PI block appeared to dominate the thermo-rheological complexity of the PI block. For a test of this molecular picture, a PI/PtBS blend having the same w_{PI} as the copolymer was utilized as a reference to reduce the copolymer data at an iso-relaxation-time (*iso*-τ_s) state defined for the Rouse segment of PI in the copolymer and bulk systems. It turned out that the dielectric data of the copolymer at low T were close to literature data for star-branched bulk PI, while the copolymer data at high T were close to the data expected for a linear bulk PI chain having the type-A dipole only in a portion of its backbone and feeling an extra friction due to the other portion (corresponding to PtBS). These results lent support to the above molecular picture. The slow dynamics of the copolymer was dominated by the PtBS block and thus exhibited thermo-rheological complexity weaker than that of the PI block.

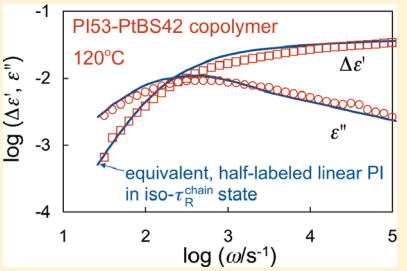

1. INTRODUCTION

It is well-known that the miscible polymer blends still have a local, frictional heterogeneity in their segmental length scale due to the chain connectivity, dynamic concentration fluctuation, and a difference of inherent motional barrier within the chain backbone of each component chain.[1−7] This local heterogeneity is responsible for many kinds of characteristic behavior of miscible polymer blends such as a wide glass transition zone, broadening of segmental relaxation mode distribution, and the thermo-rheological complexity of this distribution.

This molecular picture can be extended to disordered diblock copolymers by considering an effect(s) of the block junction on the dynamic heterogeneity. Comparison of the dynamic behavior of the disordered diblock copolymer and the corresponding miscible polymer blend enables us to elucidate this junction effect. Blends of *cis*-polyisoprene (PI) and poly(vinyl ethylene) (PVE) exhibit a lower critical solution temperature (LCST) but have a considerably wide miscibility window, and PI−PVE copolymers and PI/PVE blends have been used as model systems for studying the junction effect. PI has both of the type-A and type-B dipoles parallel and perpendicular to the chain backbone, respectively, while PVE has only type-B dipoles. Thus, the segmental (glassy) relaxation of PI and PVE as well as the global relaxation of PI block/chain can be dielectrically detected. Experiments revealed that PI−PVE diblock copolymers and the corresponding PI/PVE blends having the same PI content exhibit almost identical DSC traces and the segmental mode distribution.[8−13] This result indicates a similarity of the segmental dynamics for the PI−PVE copolymer and PI/PVE blends, i.e., lack of the junction effect on the segmental dynamics. This lack can be related to a fact that most of the segments are too far from the block junction/chain ends to be influenced by the junction/chain ends.[8,12,13] (The junction effect is enhanced by increasing the number of blocks and decreasing the block length.[14,15])

In contrast, the global dynamics over the chain/block dimension is quite different for the PI−PVE copolymers and PI/PVE blends. For the PI/PVE blends, the dynamic heterogeneity in the

Received: November 15, 2010
Revised: January 18, 2011
Published: February 18, 2011

segmental scale always results in different temperature dependence of the global relaxation processes of the components so that the thermo-rheological complexity (failure of time−temperature superposition) prevails for the terminal relaxation of the blend.[1,3,9,13,16−19] In contrast, the superposition *approximately* works for the viscoelastic modulus G^* of the PI−PVE copolymers in the terminal regime,[8,9,12] leading to a qualitative interpretation that the block junction forces the PI and PVE blocks to relax cooperatively. Nevertheless, Kornfield and co-workers[8] observed that the time−temperature shift factor for G^* of the PI−PVE copolymer does not give the superposition of the rheo-optical data (partly because the isochronal anisotropies of the components are averaged with different weights for the modulus and rheo-optical data). Furthermore, Urakawa and co-workers[9] observed that the dielectric loss ε'' at low frequencies, exclusively detecting the global motion of the PI block, cannot be superposed with the shift factor determined for G^*. Thus, rigorously speaking, the PI−PVE copolymers exhibit the thermo-rheological complexity. However, this complexity is rather weak thereby allowing G^* of the copolymer to be superposed approximately. (This junction effect for the disordered copolymers is quite different from that for ordered copolymers usually accompanied by the effect of spatial confinement.[20−23])

In relation to the behavior of the disordered copolymers mentioned above, we expect that distinct thermo-rheological complexity prevails even for the diblock copolymer *if* the temperature dependence of the local mobility is significantly different for the constituent blocks. This difference would allow one block (exhibiting the stronger dependence) to relax much more slowly compared to the other block at low T. Then, the slow block would effectively behave as an immobilized anchor for the fast block thereby forcing the latter to relax as a tethered chain. In contrast, at high T, the relaxation rate should become rather similar for the two blocks thereby forcing them to relax cooperatively and behave as a free (nontethered) linear chain as a whole. Thus, the large difference of the temperature dependence of the block mobilities would result in a crossover between these types of relaxation (*crossover of the motional modes*), which should be observed as the thermo-rheological complexity not only for terminal relaxation of the copolymer chain as a whole but also for the relaxation of respective blocks.

As candidates of such blocks, we can focus on PI and poly(*p-tert*-butylstyrene) (PtBS). PI and PtBS exhibit the LCST-type phase behavior but have a surprisingly wide miscible window.[24−26] (Phase separation occurs only at inaccessibly high $T > 250$ °C[25] if PI and PtBS have the molecular weights $M \cong 10^5$.) Furthermore, PI and PtBS have very different glass transition temperatures in bulk state, $T_{g,PI}^{bulk} \cong -70$ °C and $T_{g,PtBS}^{bulk} \cong 150$ °C.[24−26] This difference of T_g^{bulk}, much larger than that for a pair of PI and PVE (cf. $T_{g,PVE}^{bulk} \cong 0$ °C), results in a significant difference of effective T_g of PI and PtBS in their miscible blends, as confirmed from viscoelastic[26] and thermal[26,27] tests. In addition, we can selectively observe the global relaxation of PI with the dielectric method because PtBS has no type-A dipole. Thus, a PI−PtBS copolymer serves as a good model material for studying the thermo-rheological behavior of the constituent blocks.

In relation to this choice of the model material, we should remember a characteristic feature of PI/PtBS blends examined previously:[25,26] In these blends, PI was the fast component and its terminal relaxation exhibited the thermo-rheological complexity being related to the spatial heterogeneity of the concentration C_{PtBS} of the slow component, PtBS. Namely, in those blends, C_{PtBS} was larger than the overlapping concentration C_{PtBS}^* only by a factor of $\cong 2$ and thus C_{PtBS} had a considerable dynamic fluctuation. This fluctuation was effectively quenched in the time scale of the global relaxation of PI thereby giving a spatial frictional heterogeneity for this relaxation. Then, some PI chains (minority) are located in a PtBS-rich region to feel a higher friction compared to the other PI chains (majority). A difference of the relaxation times of the minority and majority changed with T, which naturally resulted in the thermo-rheological complexity of the whole ensemble of the PI chains.

As for the PI−PtBS diblock copolymer examined in this paper, the global relaxation of the PI block should be affected by not only the PI−PtBS junction but also the frictional heterogeneity explained above. We need to separate these effects and focus on the junction effect. The PI/PtBS blend having the same composition and component molecular weights as the PI−PtBS copolymer serves as a reference system for specifying the frictional heterogeneity for the PI blocks: The concentration fluctuation giving this heterogeneity should be less significant for the copolymer than for the blend[28] and the blend and copolymer are not thermodynamically equivalent. Thus, the thermo-rheological complexity seen for the reference blend can be regarded as the upper bound complexity for the copolymer due to the fluctuation.

Following this strategy, we have examined the viscoelastic, dielectric, and thermal behavior of a PI−PtBS diblock copolymer and the PI/PtBS reference blends. It turned out that the dielectrically detected global relaxation of the PI block exhibited the thermo-rheological complexity due mainly to the junction effect, i.e., the crossover of the motional modes for the PI block with T explained earlier. The viscoelastic data of the copolymer exhibited the complexity weaker than that for the PI block. Details of these results are presented/discussed in this paper.

2. EXPERIMENTAL SECTION

2.1. Materials. A *cis*-polyisorene−poly(*p-tert*-butylstyrene) (PI53−PtBS42) diblock copolymer and a PI homopolymer (PI53) were anionically synthesized with *sec*-butyllithium (initiator) in benzene at 35 °C. In the synthesis of the copolymer, the PtBS block anion was polymerized first and split into two portions, one being terminated with methanol to recover the precursor PtBS sample, and the other being copolymerized with isoprene monomer to give the desired PI−PtBS diblock sample.

These samples were characterized with GPC (CO-8020 and DP-8020, Tosoh) equipped with a refractive index (RI)/low-angle light scattering (LALS) monitor (LS-8000, Tosoh Co.) and a ultraviolet (UV) adsorption monitor (UV-8020). The weight-average molecular weight M_w and polydispersity index M_w/M_n of the PtBS42 precursor were determined from the LALS/RI signals, with a previously characterized PtBS70 sample[25] ($10^{-3}M_w = 69._5$) being utilized as a LALS/RI reference. The PI content w_{PI} (= 55.7 wt %) of the PI53−PtBS42 sample was determined from the RI/UV signals, with the PtBS70 sample and the previously used monodisperse PI standards[29−31] being utilized as RI/UV references. The molecular weight of the PI block of the copolymer was evaluated from this w_{PI} and the precursor PtBS42 molecular weight $M_{w,PtBS}$ as $M_{PI} = w_{PI}M_{w,PtBS}/(1 - w_{PI})$ ($= 52._6 \times 10^3$), and the polydispersity index of the copolymer was evaluated from elution volume calibration made with the monodisperse PI standards. The molecular weight and polydispersity index of the PI53 homopolymer sample were determined from the elution volume calibration.

The characteristics of all these samples are summarized in Table 1, with the sample code number representing the molecular weight in units of 1000. (Note that the amounts of the monomer and initiator utilized for the synthesis were carefully adjusted to match the molecular weight of PI53 homopolymer ($M_{PI} = 53._4 \times 10^3$) with that of the PI block.) The microstructure determined from ^{1}H NMR (Varian MERCURYplus

Table 1. Characteristics of Samples

code	$10^{-3}M_{PI}$	$10^{-3}M_{PtBS}$	M_w/M_n
PI53−PtBS42	$52._6$	$41._8$	1.08
PI53	$53._4$		1.03
PtBS42[a]		$41._8$	1.04

[a] Precursor of PI53−PtBS42 copolymer.

AS400) were the same for the PI53 sample and the PI53 block of the copolymer, 1,4-*cis*:1,4-*trans*:3,4 = 78:14:8. This microstructure, very close to that of the previously utilized PI20 (1,4-*cis*:1,4-*trans*:3,4 = 79:14:7),[26] allowed the PI53 chain/block to be miscible with the PtBS42 chain/block in a wide range of T.

The materials subjected to thermal, viscoelastic, and dielectric measurements were the PI53−PtBS42 copolymer and a blend of PtBS42 (precursor of copolymer) with PI53. The PI content in the blend was set identical to that of the copolymer, w_{PI} = 55.7 wt %. The blend, utilized as the reference material for the copolymer, was prepared according to the previously reported method:[24] The prescribed masses of PI and PtBS were dissolved in tetrahydrofuran (THF) at a total concentration of 10 wt % and then precipitated in a dropwise way into an excess methanol/acetone (8/2 wt/wt) mixture vigorously stirred by a magnetic bar. The blends were recovered *via* decantation and thoroughly dried under vacuum first at room temperature and then at 125 °C. The blends thus prepared were transparent, which was in accord with the PI/PtBS miscibility.[24,25]

2.2. Measurements. Linear viscoelastic, dielectric, and thermal (differential scanning calorimetry, DSC) measurements were conducted for the PI53−PtBS42 diblock copolymer as well as the PI53/PtBS42 reference blend, both having a PI content of w_{PI} = 55.7 wt %. The measurements were also conducted for the components of the blends, PI53 and PtBS42, in their respective bulk states. The viscoelastic and dielectric data of these components are summarized in Appendix A.

The linear viscoelastic measurements were conducted with a laboratory rheometer (ARES, TA Instruments) at temperatures $20 \le T/°C \le 120$. A parallel-plate fixture with a diameter of 8 mm was utilized. The oscillatory strain amplitude was kept small ($\gamma_0 \le 0.1$) to ensure the linearity of the storage and loss moduli G' and G'' measured as functions of the angular frequency ω.

The dielectric measurements (in the linear response regime) were conducted also at $20 \le T/°C \le 120$. The samples were charged in a dielectric cell composed of parallel-plate electrodes and a guard electrode. The measurements were made with an impedance analyzer/dielectric interface system (1260 and 1296, Solartron) and a capacitance bridge (1615A, QuadTech). In this paper, the dielectric data obtained at frequencies $f \le 10^6$ Hz are presented as plots against the angular frequency, $\omega = 2\pi f$.

The DSC measurements were conducted with a laboratory calorimeter (DSC Q20; TA Instruments). The DSC traces were recorded for respective specimens (10−15 mg for each) at a heating rate of 10 °C/min in a range of T between −120 and +250 °C.

3. RESULTS

3.1. Overview of Thermal Behavior. Figure 1 shows the DSC profiles measured for the PI53−PtBS42 copolymer and the PI53/PtBS42 reference blend having the same M_{PI}, M_{PtBS}, and w_{PI} (=55.7 wt %; volume fraction ϕ_{PI} = 0.59 as evaluated on the basis of an assumption of volume additivity). For comparison, the profiles are shown also for the PI53 and PtBS42 bulk samples. The horizontal dashed lines indicate the high-T baselines. The thin arrows indicate the glass transition temperatures $T_{g,PI}^{bulk}$ (=−65 °C) and $T_{g,PtBS}^{bulk}$ (=147 °C) for bulk PI53 and PtBS42.

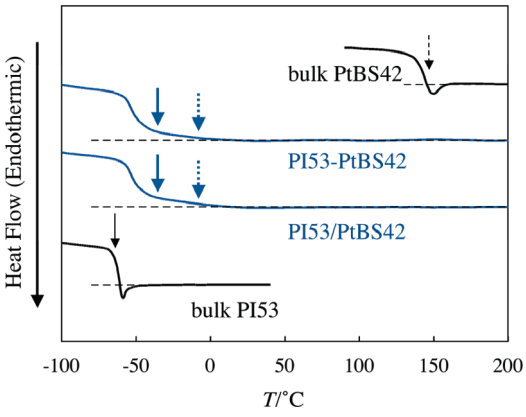

Figure 1. DSC traces for the PI53−PtBS42 diblock copolymer and the PI53/PtBS42 blend. Thin solid and dashed arrows denote the glass transition temperature of bulk PI53 ($T_{g,PI}^{bulk}$ = −65 °C) and bulk PtBS42 ($T_{g,PtBS}^{bulk}$ = 147 °C), respectively. The thick solid and dotted arrows, respectively, show the effective $T_{g,PI}^{eff}$ and $T_{g,PtBS}^{eff}$ of the Rouse segments of PI and PtBS in the blends/copolymer expected from the WLF analysis shown in Appendix B.

The thick arrows indicate effective T_g^{eff} in the blend explained later.

Figure 1 clearly indicates that the PI53−PtBS42 copolymer and the PI53/PtBS42 reference blend exhibit similarly broad, almost two-step glass transitions. This transition occurs in a range of T well below $T_{g,PtBS}^{bulk}$ because of significant plasticization of PtBS due to PI. The broadness of the transition reflects a broad distribution of local frictional environment for the monomeric segments due to the dynamic heterogeneity, as noted for a variety of miscible blends and disordered diblock copolymers.[1−9,12,26,27] The similarity of the glass transition behavior of the PI53−PtBS42 copolymer and PI53/PtBS42 blend demonstrates a similarity of the dynamics of the monomeric segments therein, as noted also for PI−PVE copolymers and PI/PVE blends.[8,9,12]

In Figure 1, the thick solid and dotted arrows indicate effective $T_{g,PI}^{eff}$ (=−35 °C) and $T_{g,PtBS}^{eff}$ (=−8 °C) of the PI and PtBS components in the blend estimated from the Williams−Landel−Ferry (WLF) analysis[32] of the viscoelastic/dielectric data at high $T \gg T_g^{eff}$ (shown later in Figure 2). The method of this analysis, fully explained in the previous paper,[26] is summarized in Appendix B. Those high-T data reflect the rubbery (global) relaxation process of PI and PtBS and thus the T_g^{eff} obtained from the analysis is related to the dynamics of the smallest motional unit for this process, i.e., the Rouse segment, not the monomeric segment exhibiting the thermal behavior in Figure 1. The dynamics of the monomeric segment of PI in the glassy matrix of PtBS at *low* $T < (T_{g,PtBS}^{eff})$, characterized by the Arrhenius behavior, differs considerably from the WLF-type dynamics of the Rouse segments at *high* T ($> T_{g,PtBS}^{eff}$), as can be noted from a recent study by Ediger and co-workers.[27] This difference possibly results in a moderate difference between the $T_{g,PI}^{eff}$ (=−35 °C) and a characteristic temperature for the onset of endothermic behavior (≅−50 °C), the latter being assigned as the real T_g of the monomeric segment of PI in the blend; see Figure 1. The high-T part of the thermally detected glass transition is associated with just a small change of the DSC profile and $T_{g,PtBS}^{eff}$ (thick dotted arrow) is located at the edge of this high-T part, which can be again related to the difference between the Rouse and monomeric segments of PtBS. (One may also like to compare a characteristic length ξ for motion of the two types of segments.

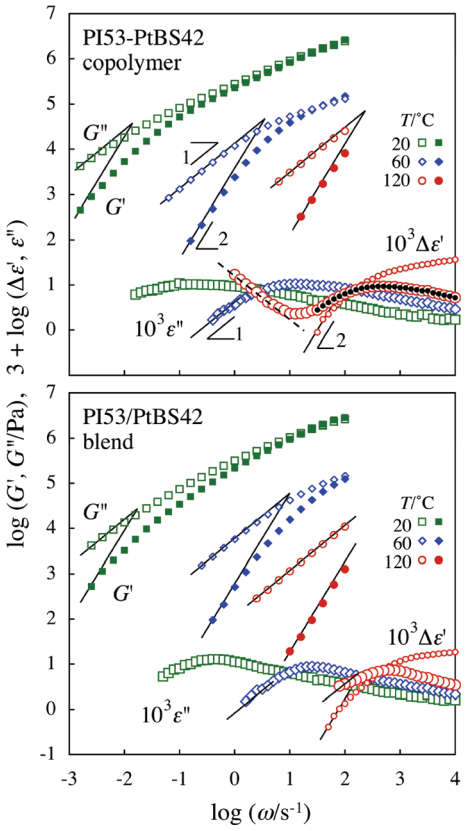

Figure 2. Viscoelastic and dielectric behavior of PI53−PtBS42 diblock copolymer and PI53/PtBS42 blend. For the dielectric data of PI53−PtBS42 at 120 °C (top panel), the large unfilled circle, dotted line, and small filled circles indicate the raw ε'' data, the contribution of the direct current (dc) conduction ε_{dc}'', and the residue $\varepsilon'' - \varepsilon_{dc}''$. This study utilized only the raw ε'' data at moderately high ω where the dc conduction negligibly contributed to the data.

Quasielastic neutron scattering experiments[33,34] showed that different monomeric segments have different mobilities even at high T and that $\xi \cong 0.8$ nm for the monomeric segment of PI in a PI−polystyrene copolymer and the segmental correlation vanishes at length scales > ξ. In contrast, for the Rouse segment of PI (of a size $\cong$ 1 nm), the data shown in Figure 2 cover the Rouse/entanglement relaxation zone and the corresponding ξ can be close to the entanglement length a (=6.2 nm, as shown later in eq 3), or even larger. This difference of ξ is an interesting subject of research but beyond the scope of this paper focusing on the junction effect on the global dynamics of disordered copolymers.)

3.2. Overview of Viscoelastic and Dielectric Behavior. Now, we examine the viscoelastic and dielectric data reflecting the global dynamics (resulting from the motion of the Rouse segments). Figure 2 shows the angular frequency (ω) dependence of the storage and loss moduli, $G'(\omega)$ and $G''(\omega)$, of the PI53−PtBS42 copolymer and the PI53/PtBS42 reference blend. The raw data of the dielectric loss, $\varepsilon''(\omega)$, and the decrease of the dynamic dielectric constant $\varepsilon'(\omega)$ from its static value $\varepsilon'(0)$, $\Delta\varepsilon'(\omega) = \varepsilon'(0) - \varepsilon'(\omega)$, are multiplied by a factor of 10^3 and compared with the $G'(\omega)$ and $G''(\omega)$ data. For clarity of the plots, the ε'', G', and G'' data are shown only for representative T, and the $\Delta\varepsilon'$ data, only for the highest T. At high T, the ε'' data at low ω were contributed from the direct current (dc) conduction, $\varepsilon_{dc}'' = \sigma/\omega \propto \omega^{-1}$ with σ = dc conductivity; see, for example, the dashed line of slope −1 attached to the ε'' data at 120 °C in the top panel. For such cases, we examined the quality of the data by allowing σ to change by ±30% to fit the low-ω ε'' data with $\varepsilon_{dc}'' = \sigma/\omega$, subtracting this ε_{dc}'' from the raw ε'' data, and comparing the residue $\varepsilon'' - \varepsilon_{dc}''$ with the raw data. At moderately high ω, the residue was quite insensitive to the ±30% change of σ and indistinguishable from the raw data; compare the small filled circles (residue) and large unfilled circles (raw data) in the top panel. Those data have a negligible dc contribution, and this paper utilizes only the *raw data* at such moderately high ω.

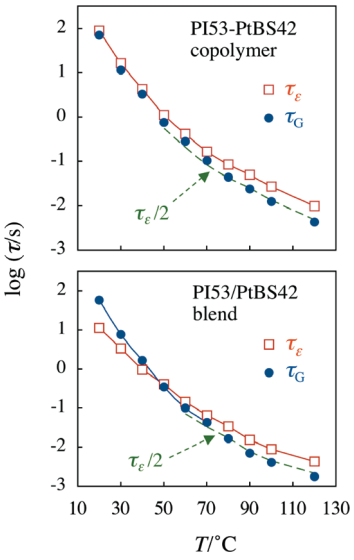

Figure 3. Comparison of the dielectric and viscoelastic terminal relaxation times, τ_ε and τ_G, obtained for the PI53−PtBS42 copolymer and the PI53/PtBS42 blend at various T. The dashed curves indicate $\tau_\varepsilon/2$.

In Figure 2, the copolymer and the blends (almost) exhibit the terminal viscoelastic and dielectric relaxation characterized with the power-law tails of the G' ($\propto\omega^2$), G'' ($\propto\omega$), $\Delta\varepsilon'$ ($\propto\omega^2$), and ε'' ($\propto\omega$) at low ω. The second-moment average (terminal) viscoelastic and dielectric relaxation times,[23] τ_G and τ_ε, were evaluated from those data as

$$\tau_G = \left[\frac{G'(\omega)}{\omega G''(\omega)}\right]_{\omega\to 0}, \quad \tau_\varepsilon = \left[\frac{\Delta\varepsilon'(\omega)}{\omega\varepsilon''(\omega)}\right]_{\omega\to 0} \qquad (1)$$

These τ_G and τ_ε values are well-defined with respect to the viscoelastic and dielectric relaxation spectra and close (though not identical) to the characteristic times of the slowest relaxation modes.[23]

The dielectric relaxation of the copolymer and blend seen in Figure 2 is exclusively attributable to the global motion of the PI component therein, either the PI block or homo-PI chain. (The relaxation of the monomeric segments of PI and PtBS occurs at high ω not covered in our experimental window.[35]) In contrast, the viscoelastic relaxation detects the global motion of the copolymer chain as a whole and/or all component chains in the blends. Thus, comparison of τ_ε and τ_G provides us with a clue for examining if PI dominates the terminal relaxation of the copolymer/blends. This comparison is made in Figure 3, where the τ_G and τ_ε data (filled circles and unfilled squares) of the copolymer and the blend are plotted against T.

We first focus on τ of the PI53/PtBS42 blend. Since the PI and PtBS chains therein are not chemically connected and can relax at different times, we may straightforwardly assign the slow component

by comparing τ_G and τ_ε. For this comparison of τ evaluated from different quantities (G^* and ε^*), we first need to note that PI53 chains are rather well entangled in the bulk state ($M_{PI53} \cong 10M_{e,PI}^{bulk}$ with $M_{e,PI}^{bulk} = 5.0 \times 10^3$).[36] These chains should be entangled also in the blends even in an *extreme* case where PtBS42 chains behave as a simple solvent to dilute the entanglements between the PI chains; $M_{e,PI}$ for this full dilution case is estimated from the PI volume fraction in the blends, $\phi_{PI} = 0.59$, as[29,30] $M_{e,PI}^{bulk}/\phi_{PI}^{1.3} = 9.9 \times 10^3 < M_{PI53}$. (Actually, the PtBS42 chains entangle with the PI chains to give $M_{e,PI}$ smaller than this estimate, as explained later.)

Thus, the behavior of entangled binary blends of linear PI is helpful for assigning the fast and slow components in the PI53/PtBS42 blend. Extensive experiments for the PI/PI blends[23,29−31,37] revealed that the viscoelastic $\tau_{G,slow}$ and dielectric $\tau_{\varepsilon,slow}$ defined for the slow component satisfy a relationship, $\tau_{G,slow}/\tau_{\varepsilon,slow} \cong 1/2$ (due to a considerable contribution of the constraint release/tube dilation mechanisms[29,30]) and these $\tau_{G,slow}$ and $\tau_{\varepsilon,slow}$ data are close to the τ_G and τ_ε data of the blends as a whole. This relationship also holds for monodisperse linear PI systems in which all chains have the same relaxation time.[31,37] In contrast, $1/2 < \tau_{G,slow}/\tau_{\varepsilon,slow}$ (≤ 1) for the fast component in the PI/PI blends.[29,30] From this behavior of PI/PI blends, we can judge that the terminal relaxation of PI in our PI/PtBS blend is slower or equally slow compared to the PtBS relaxation if $\tau_G/\tau_\varepsilon \cong 1/2$, while the PI relaxation is considerably faster than the PtBS relaxation if the τ_G/τ_ε ratio is well above 1/2, in particular in a case of $\tau_G/\tau_\varepsilon > 1$. (PtBS has no type-A dipole so that the PI/PtBS blends exhibit $\tau_G/\tau_\varepsilon \gg 1$ if PtBS relaxes much slower than PI.)

As seen in the bottom panel of Figure 3, the τ_G/τ_ε ratio for the PI53/PtBS42 blend is larger than unity and the PI relaxation is significantly faster than the PtBS relaxation at low $T \leq 50$ °C. This ratio decreases to $\cong 1/2$ and thus the PI relaxation becomes comparable to (or slower than) the PtBS relaxation at higher T. This crossover reflects a difference in the temperature dependence of the friction coefficients of the Rouse segments of the PI and PtBS chains.[25,26]

Now, we turn our attention to the PI53−PtBS42 copolymer; see the top panel of Figure 3. For the copolymer, the τ_G/τ_ε ratio is close to unity at 20 °C and decreases gradually to $\tau_G/\tau_\varepsilon \cong 1/2$ with increasing T. This behavior is qualitatively similar to but quantitatively different from the behavior of the PI53/PtBS42 blend (cf. bottom panel). This difference should reflect the connectivity between PI and PtBS blocks: The connectivity does not allow these block to relax in a *completely independent* way to have significantly different τ, although approximate independence can be realized at low T, as discussed later. For this reason, the temperature dependence becomes rather similar for τ_ε and τ_G of the copolymer, the former exclusively detecting the PI block relaxation while the latter representing the relaxation of the copolymer chain, i.e., the connected sequence of the PI and PtBS blocks.

3.3. Thermo-Rheological Behavior of PI Block. Figure 4 examines the time−temperature superposability for the $\Delta\varepsilon'$ and ε'' data of the copolymer and the blend, i.e., of the PI53 block and PI53 chain therein. The reference temperature was chosen to be $T_r = 363$ K (= 90 °C), and the data at the other temperatures were multiplied by an intensity correction factor, $b_T = T/T_r$ with T and T_r in K unit, and shifted along the ω axis by a factor $a_{T,\varepsilon}$. (A ratio of densities at T and T_r is to be included in b_T, in principle.[26] However, this ratio was safely neglected here because a change in the density with T was much smaller than the change of T itself.) The thick solid curves in the bottom panel indicate the dielectric data of bulk PI53 at its $T_{r,bulk} = 303$ K

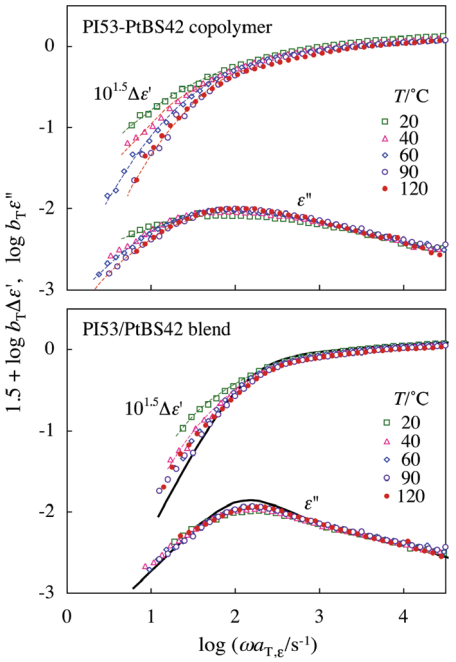

Figure 4. Test of the time−temperature superposability for the dielectric $\Delta\varepsilon'$ and ε'' data for the PI53−PtBS42 copolymer and the PI53/PtBS42 blend. These data are multiplied by the intensity correction factor $b_T = T/T_r$ (with the reference temperature of $T_r = 363$ K) and shifted along the ω axis by a factor of $a_{T,\varepsilon}$ to achieve the best superposition at $\omega > \omega_{peak}$. (The $\Delta\varepsilon'$ data are further multiplied by a factor of $10^{1.5}$ to avoid heavy overlapping with the ε'' data.) The solid curves in the bottom panel indicate the dielectric data of bulk PI53 corrected for the PI volume fraction and temperature and shifted along the ω axis to match the ε'' peak frequency. For further details, see text.

(shown in Appendix A) multiplied by the intensity correction factor $b_T^\circ = T_{r,bulk}/T_r$ and the PI volume fraction in the blend $\phi_{PI} = 0.59$, $\phi_{PI} b_T^\circ \Delta\varepsilon'_{bulk-PI}(\Lambda\omega)$ and $\phi_{PI} b_T^\circ \varepsilon''_{bulk-PI}(\Lambda\omega)$. These data are plotted against ω, with the factor $\Lambda = 0.21$ being chosen to match the ε''-peak frequencies ω_{peak} for the PI chains in the blend and bulk.

The shift factor $a_{T,\varepsilon}$ for the plots in Figure 4 was chosen in a way that the $\Delta\varepsilon'$ and ε'' data were best superposed at $\omega > \omega_{peak}$. This factor is plotted against T in the top panel of Figure 5. The $a_{T,\varepsilon}$ data are almost indistinguishable for the copolymer and the blend, confirming the similarity of the friction coefficient of the Rouse segment (smallest motional unit for the rubbery relaxation) for the PI block in the copolymer and PI chain in the blend. The $a_{T,\varepsilon}$ data of the blend are later utilized to reduce the data of the copolymer/blend to an iso-relaxation-time state defined with respect to the Rouse segment of bulk PI.

For the copolymer as well as the blend, Figure 4 clearly indicates that the slow dielectric mode distribution broadens with decreasing T and the superposition fails for the dielectric data at low $\omega < \omega_{peak}$. The broadening is more clearly noted for $\Delta\varepsilon'$ than for ε'' because slow modes are more sensitively reflected in $\Delta\varepsilon'$ than in ε''.[38] The molecular origin of this broadening is not exactly the same for the copolymer and blends, as discussed below.

For the PI/PtBS blends, the conditions necessary for the mode broadening and thermo-rheological complexity of the PI relaxation to be observed are as follows:[25,26] (1) the PtBS chains are not deeply overlapping with each other, (2) the average end-to-end distance R_{PI} of the PI chain is not much larger than R_{PtBS} of

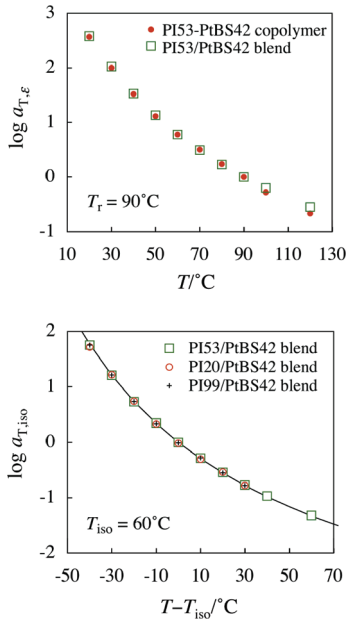

Figure 5. Top panel: Shift factor $a_{T,\varepsilon}$ utilized for superposition of the dielectric data for the PI53−PtBS42 copolymer and PI53/PtBS42 blend (cf. Figure 4). The $a_{T,\varepsilon}$ data, defined with respect to T_r = 90 °C, are plotted against T. Bottom panel: Shift factor $a_{T,iso}$ for the PI53/PtBS42 blend obtained after the CR/DTD correction for the $a_{T,\varepsilon}$ data shown in the top panel. The $a_{T,iso}$ data, defined with respect to the iso-τ_s temperature $T_{iso\text{-}PI}$ = 60 °C (that corresponds to $T_{r,bulk}$ = 30 °C for bulk PI), are plotted against $T - T_{iso\text{-}PI}$. The $a_{T,iso}$ data are also shown for the other PI/PtBS blends[51] having the same w_{PI} (= 55.7 wt %) as the PI53/PtBS42 blend. (The sample code numbers indicate 10^{-3} M.) For further details, see text.

the PtBS chain, and (3) the terminal relaxation is much faster for the PI chain than for the PtBS chain. If conditions 1 and 2 are satisfied, all PI chains cannot overlap with the PtBS chains to the same extent and thus a PI chain in a PtBS-rich region feels a larger friction compared to the other PI chains out of this region. The resulting frictional distribution among the PI chains survives in the time scale of the global PI relaxation if condition 3 is satisfied. This frictional heterogeneity naturally results in the mode broadening for the whole ensemble of the PI chains.[25,26] This molecular picture explains why the broadening is less significant for the PI53/PtBS42 blend ($C_{PtBS} \cong 3C_{PtBS}^*$)[39] than for the previously examined low-M blends ($C_{PtBS} \cong 2C_{PtBS}^*$).[26] Related broadening (resulting in bimodal distribution of relaxation times) has been noted also for low-M PI/polystyrene blends.[40]

Now, we turn our attention to the thermo-rheological behavior of the PI53−PtBS42 copolymer seen in the top panel of Figure 4. Although the global dynamics of disordered copolymers is generally affected by the concentration fluctuation that results in the frictional heterogeneity,[41] the fluctuation should be weaker[28] and the corresponding thermo-rheological complexity should be less significant for the copolymer than for the reference blend having the same composition and component molecular weights. Nevertheless, the broadening of dielectric data is more significant for our PI53−PtBS42 copolymer than for the PI53/PtBS42 blend. This observation cannot be explained from the molecular scenario explained above, because the conditions 1 and 2 are equally satisfied for these copolymer and blend while the condition (3) should be less valid for the copolymer (having $1/2 \leq \tau_G/\tau_\varepsilon \leq 1$ at any T; cf. top panel of Figure 3). Thus, the strong dielectric broadening seen for the PI block should be mainly attributed to a crossover of the motional mode of the PI block with T due to the block connectivity, as briefly explained earlier. This crossover is further discussed below.

4. DISCUSSION

4.1. Crossover of Motional Mode of PI Block with *T*. For a linear diblock copolymer in the disordered state, the motion of one block (e.g., PI block) is strongly affected by the other block (PtBS block) due to the block connectivity.[21,23,42,43] Strictly speaking, this effect of connectivity is to be represented as an internal boundary condition for the equation of motion for the copolymer chain, and the motion of the two blocks is described in terms of the eigenmodes associating this equation and thus correlated to each other. Specifically, the eigenmode relaxation times are the same but the eigenmode intensities can be different for the two blocks, as noted for homopolymer chains.[44−46] In this sense, we cannot define the "fast" and "slow" blocks for the copolymer if we only consider the eigenmode relaxation times. However, if we also consider the eigenmode intensities, we can still define the fast and slow blocks as those having small and large intensities for the slowest eigenmode. (This fact can be easily noted from a simple example for a linear homopolymer:[45] The chain end and the chain center always have the same slowest eigenmode relaxation time but the intensity of this eigenmode vanishes for the chain end. For this reason, the chain end relaxes much faster than the chain center.)

Since the effective T_g^{eff} is higher for PtBS42 than for PI53 in the copolymer as well as the blend (cf. Figure 1), a decrease of T results in stronger retardation of the PtBS42 relaxation. Thus, at low T, the PtBS42 block behaves as the slow block in the above sense, and the PI block would be effectively anchored by the PtBS42 block to behave as a tethered chain during the dominant part of its relaxation. In contrast, at high T, the anchoring effect of PtBS should become weaker and finally vanish because of stronger acceleration of the PtBS relaxation with increasing T. For this case, the PI and PtBS blocks would behave as portions of a free (nontethered), linear chain and relax cooperatively.

This crossover of the motional mode of the PI block, from the tethered chain like behavior at low T to the linear chain like behavior at high T, appears to be the main mechanism of the strong dielectric broadening observed for the PI block. For a test of this molecular picture, we can compare the dielectric behavior of the PI block with that of *equivalent* star-branched bulk PI (a model for tethered chain) and/or *equivalent* linear bulk PI. In the following, we first specify these equivalent star/linear chains and then make this comparison.

4.2. Equivalent Bulk PI Chain Defined for PI Block. *4.2.1. Entanglement Length.* For specifying the equivalent bulk PI chain for the PI block, we first need to know the entanglement length a ($\propto M_e^{1/2}$) for the PI block. For homopolymers, this length is well correlated with the packing length p ($\cong a/20$).[36,47,48] Considering this feature and the additivity of the chain contour length of the components in blends, we proposed a mixing rule for the packing length[26] that is rewritten for the entanglement length as[35]

$$a = n_{PI} a_{PI}^{bulk} + n_{PtBS} a_{PtBS}^{bulk} \quad (2)$$

Here, n_X (X = PI, PtBS) is the number fraction of the Kuhn segment of the component X in the blend. This mixing rule has

been tested for high-M PI/PtBS blends exhibiting the two-step entanglement plateau similar to that for PI/PI blends[29,30] and its validity has been confirmed.[35] (The high-ω entanglement plateau height, being proportional to a^{-2}, was satisfactorily described by eq 2 but was significantly underestimated by the other mixing rules such as a harmonic averaging rule[49] based on the component volume fraction.[35]) From the data of the Kuhn molecular weights M_{Kuhn} ($\cong$130 for PI[36] and $\cong$1500 for PtBS[50]), the n values in the PI/PtBS blend with w_{PI} = 55.7 wt % were obtained to be n_{PtBS} = 0.06, n_{PI} = 0.94. From these values and the a^{bulk} data (=5.8 and 11.7 nm for PI and PtBS),[36] eq 2 gives

$$a = 6.2 \text{ nm } (\cong 1.07 a_{PI}^{bulk}) \quad \text{for PI/PtBS with } w_{PI} = 55.7 \text{ wt\%} \tag{3}$$

This a is common for all components in the PI/PtBS blend and PI−PtBS copolymer.

The a value given by eq 3 is considerably smaller than the $\langle R_{PtBS}^2\rangle^{1/2}$ and $\langle R_{PI}^2\rangle^{1/2}$ values for the PtBS42 and PI53 chains (= 12.3 and 19.0 nm evaluated from empirical equations;[36] $\langle R_{PtBS}^2\rangle/\text{nm}^2 = 3.6_1 \times 10^{-3} M_{PtBS}$ and $\langle R_{PI}^2\rangle/\text{nm}^2 = 6.7_9 \times 10^{-3} M_{PI}$). Thus, the PtBS42 and PI53 chains are mutually constraining the large-scale motion (i.e., entangled), despite the PtBS42 molecular weight is close to M_e of bulk PtBS (= 37.6×10^3).

4.2.2. Relaxation Time of Rouse Segment. For comparison of the dielectric data for the PI block and the equivalent bulk PI chain, we need to specify the relaxation time τ_s of the Rouse segment, the smallest motional unit during the rubbery relaxation process. This τ_s can be analyzed in the following way.

The terminal relaxation time of *entangled* chains, τ, is generally expressed in terms of τ_s, the chain molecular weight M, and the entanglement molecular weight M_e as $\tau = \tau_s F(M, M_e)$ with F being the structural factor. The functional form of F changes with the mode of chain motion. For example, $F \propto M^3/M_e$ for the pure reptation mode, while $F \propto M^{3.5}/M_e^{1.5}$ for the reptation mode combined with the contour length fluctuation, constraint release (CR), and dynamic tube dilation (DTD).[37]

If the mode of chain motion does not change with T, a change of τ data with T can be exclusively attributed to a change of τ_s. This is the case for chemically uniform blends. However, in the PI/PtBS blend, a ratio of the relaxation times of the PI and PtBS chains changes with T. This change leads to some change of the CR/DTD contribution to the PI relaxation[26] thereby affecting the functional form of the structural factor F. The shift factor $a_{T,\varepsilon}$ obtained from the dielectric data of the PI/PtBS blend (cf. top panel of Figure 5) is equivalent to a ratio of the dielectric τ_ε of the PI chains at T and T_r and reflects not only the change of τ_s but also a change of the CR/DTD contribution to the PI relaxation, although the latter change is minor.[26] The change of CR/DTD contribution can be corrected with a method reported previously[26] and briefly explained in Appendix B1. The $a_{T,\varepsilon}$ data after this correction exclusively represent the change of τ_s with T. The WLF analysis of those data indicated that the iso-τ_s temperature $T_{iso\text{-}PI}$ defined for the Rouse segment is higher, by $\Delta T_{iso\text{-}PI}$ = 30 °C, for PI in the PI/PtBS blends (w_{PI} = 55.7 wt %) than for bulk PI; cf. Appendix B1.

In the bottom panel of Figure 5, the shift factor $a_{T,iso}$ for the PI53/PtBS42 blend defined with respect to $T_{iso\text{-}PI}$ = 60 °C is plotted against $T - T_{iso\text{-}PI}$ (squares). For comparison, $a_{T,iso}$ is shown for the other PI/PtBS blends with the *same* composition (w_{PI} = 55.7 wt %) examined elsewhere;[51] the sample code number indicates $10^{-3}M$. The solid curve shows the WLF equation describing the a_T data for bulk PI, $\log a_T = -4.425(T - T_{r,bulk})/(140.0 + T - T_{r,bulk})$ with $T_{r,bulk} = T_{iso-PI}^{bulk}$ = 30 °C (cf. Appendix A). The excellent agreement of the plots and the curve is indicative of the reliability of our WLF analysis. Furthermore, the plots are indistinguishable for the blends having the same w_{PI}, indicating that τ_s of the Rouse segment is *locally* determined just by the PI/PtBS composition. Thus, the PI53−PtBS42 copolymer and the PI/PtBS blends having the same w_{PI} should have the same τ_s, and an iso-τ_s relationship holds for the Rouse segments of PI in these copolymer/blends and in bulk PI:[52]

$$\tau_s^{\text{bulk PI}}(T) = \tau_s^{\text{PI in b/c}}(T + \Delta T_{\text{iso-PI}}), \quad \frac{\zeta_s^{\text{bulk PI}}(T)}{T} = \frac{\zeta_s^{\text{PI in b/c}}(T + \Delta T_{\text{iso-PI}})}{T + \Delta T_{\text{iso-PI}}} \tag{4}$$

where ζ_s denotes the friction coefficient of the Rouse segment, the superscript "PI in b/c" stands for PI in the blend/copolymer systems, and $\Delta T_{iso\text{-}PI}$ = 30 K.

An *effective* glass transition temperature of PI53 in the blends, defined for the Rouse segment of PI through the WLF relationship (cf. Appendix B1), is expected to be higher, by $\Delta T_{iso\text{-}PI}$, than $T_{g,PI}$ (= −65 °C) of bulk PI53. This $T_{g,PI}^{eff}$ (= −35 °C), shown with the thick solid arrows in Figure 1, is located at the low-T side of the broad glass transition zone of the blend and copolymer, as expected. (At the same time, we should again emphasize that the thermally detected glass transition is related to motion of the monomeric segments and real T_g of these segments is moderately lower than $T_{g,PI}^{eff}$ estimated from the high T data reflecting the motion of the Rouse segments, as explained earlier.)

A comment needs to be made for $T_{iso\text{-}PI}$ = 60 °C of the blend that corresponds to T_{iso-PI}^{bulk} = 30 °C. Since the $a_{T,\varepsilon}$ data were obtained from the superposition of the ε'' data at $\omega \geq \omega_{peak}$ (cf. Figure 4), the $T_{iso\text{-}PI}$ evaluated from those data is the iso-τ_s temperature for the majority of PI in the blend giving the ε'' peak. The minority of PI, existing due to the concentration fluctuation, should have $T_{iso\text{-}PI}$ > 60 °C. However, the minority is rather dilute to hardly disturb the superposition of the ε'' data for the blends at $\omega \geq \omega_{peak}$. Since the fluctuation is less significant for the copolymer than for the blend,[28] we do not consider the minority in our later analysis for the copolymer.

4.2.3. Equivalent Star PI Defined for PI Block at Low T. The PI block appears to behave as the tethered chain at low T. For this PI block, we define an *equivalent star PI* as the bulk star PI having the *same* entanglement number N_e per arm ($N_e \propto M_{arm}/a^2$) as the PI block. We compare the dielectric data of the equivalent star PI and the PI block in the *iso-τ_e condition* where they have the same relaxation time τ_e of the entanglement segment. This choice of the condition is reasonable because the entanglement segment is regarded as the motional unit for the global relaxation of entangled chains. τ_e is related to τ_s of the Rouse segment (smallest motional unit for the rubbery relaxation) as $\tau_e = \tau_s N_R^2$, where N_R is the number of the Rouse segments per entanglement segment.

From the entanglement length a for the PI block (eq 3), the arm molecular weight of the equivalent star PI is specified to be

$$M_{arm} = \left(\frac{a_{PI}^{bulk}}{a}\right)^2 M_{\text{PI block}} = 46._0 \times 10^3 \text{ for equivalent star PI} \tag{5}$$

The iso-τ_s temperature for this star PI defined with respect to the PI block at a temperature T is the same as that for the PI chains in

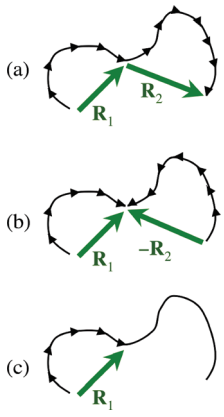

Figure 6. Schematic illustration of (a) ordinary PI having the type-A dipoles aligned along the chain backbone in the same direction from one end to the other, (b) a special class of PI having once-inverted dipoles, and (c) hypothetical PI having the type-A dipole only in a portion of the backbone.

the PI/PtBS blends (w_{PI} = 55.7 wt %) explained earlier: $T^{bulk}_{iso\text{-}PI} = T - \Delta T_{iso\text{-}PI} = T - 30$ °C (cf. eq 4). Since the comparison of the equivalent star PI and the PI block is to be made in the iso-τ_e state, the dielectric data for the latter at T, $\varepsilon_{PI\ block}^*(\omega;T)$, are not to be directly compared with the data for the former at the iso-τ_s temperature, $\varepsilon_{star}^*(\omega;T^{bulk}_{iso\text{-}PI})$, because of a difference of N_R ($\propto a^2$) for the copolymer and bulk PI: We need to make a minor shift for the frequency of the equivalent star PI by a factor of $\lambda = (N_R^{PI\ block}/N_R^{star})^2 = (a/a_{PI}^{bulk})^4 = 1.3$ ($a/a_{PI}^{bulk} = 1.07$; cf. eq 3) and compare the $\varepsilon_{PI\ block}^*(\omega;T)$ data with the shifted $\varepsilon_{star}^*(\lambda\omega; T^{bulk}_{iso\text{-}PI})$ data.

Now, we focus on the actual comparison. In literature,[31] we find the dielectric data for a series of 6-arm bulk star PI samples of various M_{arm}. Among these chains, the star PI sample of $M_{arm} = 59.0 \times 10^3$ (hereafter referred to as PI$(59)_6$) is the closest, in the M_{arm} value, to the equivalent star PI specified above (cf. eq 5). Thus, we compare the $\varepsilon_{PI\ block}^*(\omega;T)$ data of the PI block with the $\varepsilon_{PI(59)_6}$ data of PI$(59)_6$ corrected for the difference of M_{arm} (and of a):

$$\varepsilon_{eqv}^*(\omega;T) \equiv \phi_{PI} b_T \varepsilon_{PI(59)_6}^*(r_\tau \lambda\omega; T^{bulk}_{iso\text{-}PI}) \quad \text{with}$$

$$r_\tau = \frac{\tau_\varepsilon^{eqv\text{-}star}}{\tau_\varepsilon^{PI(59)_6}} = 0.11 \qquad (6)$$

Here, the PI volume fraction ϕ_{PI} (= 0.59) and the temperature factor $b_T = T^{bulk}_{iso\text{-}PI}/T$ ($T^{bulk}_{iso\text{-}PI}$ and T in K unit) are multiplied to $\varepsilon_{PI(59)6}^*$ for correction of the dielectric intensity difference between the PI$(59)_6$ sample and the PI block. The M_{arm}-correction factor, r_τ, was evaluated from the empirical equation for star PI shown in Appendix C, $\tau_\varepsilon \propto M_{arm}^{1.5} \exp\{1.4 \times 10^{-4} M_{arm}\}$. The result of this comparison is later shown in Figures 7 and 8.

4.2.4. Equivalent Linear PI Defined for PI−PtBS Copolymer at High T. At high T, the PI block appears to behave as a portion of a free linear chain and move cooperatively with the PtBS block. Thus, we define an *equivalent linear PI* as the bulk PI chain having the same entanglement number N_e as the PI−PtBS copolymer, not just the PI block. Since the entanglement length a (= 6.2 nm; eq 3) is common for the PI and PtBS block (as discussed in relation to the cooperative Rouse equilibration),[35] N_e is evaluated from the mean square end-to-end distance of the copolymer,

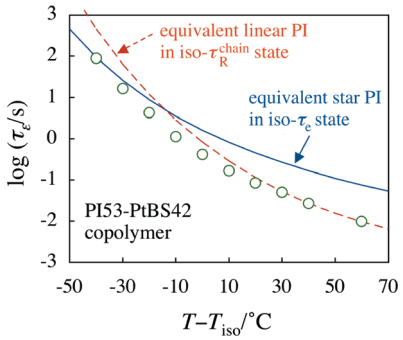

Figure 7. Comparison of the τ_ε data of PI53−PtBS42 copolymer at various T (circles) with the τ_ε expected for equivalent PI, the star PI ($M_a = 46.0 \times 10^3$; solid curve) and linear PI ($M = 66.1 \times 10^3$; dashed curve). The arm of the equivalent star PI has the same entanglement number N_e as the PI53 block, while the equivalent linear PI chain has N_e being identical to N_e for the copolymer chain as a whole. The τ_ε data of the equivalent star PI are compared in the iso-τ_e state (defined for the entanglement segment), while the data of the equivalent linear PI are compared in the iso-τ_R^{chain} state (defined for the chain as a whole). For further details, see text.

$\langle R^2\rangle = \langle R_{PI53}{}^2\rangle + \langle R_{PtBS42}{}^2\rangle = 508$ nm^2 (for Gaussian conformation of the copolymer chain), as $N_e = \langle R^2\rangle/a^2 = 13.2$. The corresponding molecular weight of the equivalent linear PI is given by

$$M_{lin} = N_e M_{e,PI}^{bulk} = 66._1 \times 10^3 \quad \text{for equivalent linear PI} \qquad (7)$$

This equivalent linear PI is hereafter referred to as PI66.

Now, we need to ask a question, what the temperature for this equivalent PI66 should be when compared with the PI block at a given high T (e.g., 120 °C). At low T, the PtBS block motion is essentially frozen in the time scale of the PI block relaxation, allowing us to reasonably compare the data for the PI block and the equivalent star PI in the iso-τ_e state. However, at high T, the PtBS block moves cooperatively with the PI block to give an extra friction for the PI block motion, so that the iso-τ_e state defined just for the PI block/chain cannot be adopted as the state for the reasonable comparison. Thus, we define an iso-τ_R^{chain} state where the longest Rouse relaxation time τ_R^{chain} is the same for the PI−PtBS copolymer and the equivalent linear PI66 chain and compare the data for the PI block and PI66 chain in this state. Note that this definition matches with the definition of the iso-τ_e state at low T because the PI block and the equivalent star PI has the same N_e and the same τ_e thereby having the same τ_R^{chain} ($\propto N_e{}^2\tau_e$) in this state.

For the PI block and the equivalent linear PI66, the iso-τ_R^{chain} state is conveniently specified by a frequency shift for PI66 at the iso-τ_s temperature for PI, i.e., at T and $T^{bulk}_{iso\text{-}PI} = T - 30$ °C for the PI block and equivalent PI, respectively. In the range of Texamined, the friction coefficient of the entanglement segment of the PtBS block, $\zeta_e^{PtBS\ block}$, is larger than $\zeta_e^{PI\ block}$ of the PI block/equivalent PI. Thus, we may utilize the Stockmayer-Kennedy (SK)[53] model for a bead−spring block chain, applicable to disordered and unentangled block copolymers,[43] to evaluate a τ_R^{chain} ratio for the PI53−PtBS42 copolymer at T and the equivalent PI66 chain at $T^{bulk}_{iso\text{-}PI}$. Utilizing the entanglement segments of the PI and PtBS blocks having the same a as the

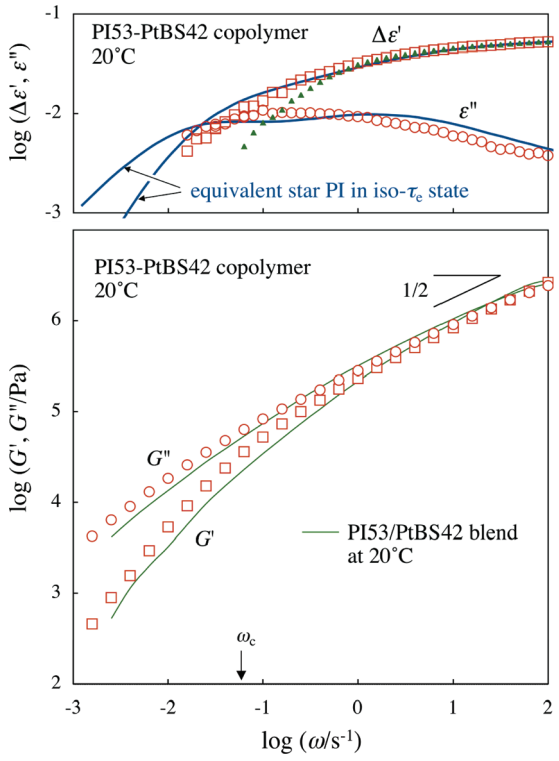

Figure 8. Top panel: Comparison of the dielectric $\Delta\varepsilon'$ and ε'' data for the PI53−PtBS42 copolymer at 20 °C (unfilled symbols) and the equivalent star PI (M_{arm} = 46.0 × 10^3; solid curves) having the arm entanglement number identical to that for the PI53 block. The comparison is made in the iso-τ_e state defined for the entanglement segment of PI. The filled triangles show the $\Delta\varepsilon'(\omega)$ data of the PI53/PtBS42 blend at 20 °C (in the iso-τ_e state). For clear comparison, this $\Delta\varepsilon'(\omega)$ plot is slightly shifted upward in the double logarithmic scale so that it agrees with the $\Delta\varepsilon'(\omega)$ plot for the copolymer (unfilled squares) at the highest ω in the panel. Bottom panel: Comparison of the viscoelastic G' and G'' data for the PI53−PtBS42 copolymer (unfilled symbols) and the PI53/PtBS42 blend (curves) at 20 °C. The arrow indicates a characteristic frequency ω_c below which the PtBS block exhibits significant motion/relaxation.

beads in the SK model, we find the viscoelastic τ_R^{chain} of the copolymer to be given by[53]

$$\tau_R^{chain} = \frac{a^2 \zeta_e^{PtBS\ block} N_e^2}{6k_B T} \frac{1}{\beta^2} \quad \text{with } N_e = N_e^{PtBS} + N_e^{PI} \tag{8}$$

Here, N_e^X (=$\langle R_X^2\rangle/a^2$) is the number of entanglement segments (beads) per X block (X = PtBS, PI), and β is the smallest eigenvalue determined from

$$L^{1/2} \tan \beta\theta = -\tan \frac{\beta(1-\theta)}{L^{1/2}} \tag{9a}$$

with

$$L = \frac{\zeta_e^{PtBS\ block}}{\zeta_e^{PI\ block}} \text{ and}$$

$$\theta = \frac{N_e^{PtBS}}{N_e} = \frac{\langle R_{PtBS42}^2\rangle}{\langle R_{PtBS42}^2\rangle + \langle R_{PI53}^2\rangle} = 0.30 \tag{9b}$$

The friction coefficient ratio L is straightforwardly evaluated from the viscoelastic data of bulk PI and PtBS, as explained in Appendix C: For example, L = 16.3 for the PI53−PtBS42 copolymer at T = 120 °C. From the $L(T)$ value thus obtained, we solved eq 9a numerically to calculate $\beta(T)$.

The Rouse relaxation time of the equivalent PI66 chain at $T_{iso\text{-}PI}^{bulk}$ is given by $\tau_R^{PI66}(T_{iso\text{-}PI}^{bulk}) = \zeta_e^{bulk\ PI}\{a_{PI}^{bulk}\}^2 N_e^2/6\pi^2 k_B T_{iso-PI}^{bulk}$. Considering a relationship $\zeta_e^{bulk\ PI} = N_R^{bulk\ PI}\zeta_s^{bulk\ PI}$ and eq 4 (iso-τ_s relationship), we can express this relaxation time as $\tau_R^{PI66}(T_{iso\text{-}PI}^{bulk}) = \zeta_e^{PI\ block}\{a_{PI}^{bulk}\}^4 N_e^2/6\pi^2 k_B T a^2$. From this expression and eq 8, a ratio of $\tau_R^{PI-PtBS}$ of the PI53−PtBS42 copolymer at T to τ_R^{PI66} at $T_{iso\text{-}PI}^{bulk}$ is given by

$$\lambda' = \frac{\tau_R^{PI\text{-}PtBS}(T)}{\tau_R^{PI66}(T_{iso\text{-}PI}^{bulk})} = \frac{\pi^2 \zeta_e^{PtBS\ block}}{\beta^2 \zeta_e^{PI\ block}} \lambda \quad \text{with}$$

$$\lambda = \left(\frac{a}{a_{PI}^{bulk}}\right)^4 (= 1.3) \tag{10}$$

From the above results, the comparison in the iso-τ_R^{chain} state can be made for the $\varepsilon_{PI\ block}^*(\omega;T)$ data of the PI53−PtBS42 copolymer at T and the $\varepsilon_{PI66}^*(\lambda'\omega;T_{iso\text{-}PI}^{bulk})$ data of the equivalent PI66 at $T_{iso\text{-}PI}^{bulk} = T - \Delta T_{iso\text{-}PI}^{bulk} = T - 30$ °C. However, for actual comparison, we need to consider two more points, the lack of the type-A dipole in the PtBS block and the molecular weight of an available PI sample, as explained below.

4.2.5. Lack of the Type-A Dipole in the PtBS Block. Ordinary linear PI chains have the type-A dipoles parallel along the chain backbone. Thus, their polarization **P** is proportional to the end-to-end vector $\mathbf{R} = \mathbf{R}_1 + \mathbf{R}_2$, where $\mathbf{R}_1$ is a vector connecting one end of the chain to a given segment and $\mathbf{R}_2$ is a vector connecting this segment to the other end; see Figure 6a. For a special class of PI chains having the dipoles once inverted at the given segment, **P** is proportional to $\mathbf{R}_1 - \mathbf{R}_2$; see Figure 6b. We can further consider a *hypothetical* PI chain that has the type-A dipoles only in one block, as schematically shown in Figure 6c. This hypothetical PI, having $\mathbf{P} \propto \mathbf{R}_1$, corresponds to the PI−PtBS copolymer having no type-A dipole in the PtBS block. For all these PI chains, the normalized dielectric relaxation function $\Phi(t)$ (= 1 at t = 0) is given by the autocorrelation of **P** and can be expressed as[23,37]

$$\text{ordinary PI: } \Phi_{ord}(t) = \frac{\langle\{\mathbf{R}_1(t) + \mathbf{R}_2(t)\}\cdot\{\mathbf{R}_1(0) + \mathbf{R}_2(0)\}\rangle}{\langle \mathbf{R}^2\rangle} \tag{11}$$

$$\text{dipole-inverted PI: } \Phi_{inv}(t) = \frac{\langle\{\mathbf{R}_1(t) - \mathbf{R}_2(t)\}\cdot\{\mathbf{R}_1(0) - \mathbf{R}_2(0)\}\rangle}{\langle \mathbf{R}^2\rangle} \tag{12}$$

$$\text{hypothetical PI: } \Phi_{part}(t) = \frac{\langle \mathbf{R}_1(t)\cdot\mathbf{R}_1(0)\rangle}{\langle \mathbf{R}_1^2\rangle} \tag{13}$$

Here, $\langle ...\rangle$ indicates the average at equilibrium. (In the denominator of eqs 11 and 12, we have considered the Gaussian feature of the chain, $\langle \mathbf{R}_1(t)\cdot\mathbf{R}_2(t)\rangle = 0$ at any time t at equilibrium.) The dielectric $\Delta\varepsilon'(\omega)$ and $\varepsilon''(\omega)$ are proportional to the sine- and cosine-Fourier transformation of $-d\Phi(t)/dt$.[23,37]

The dipole-inverted PI samples have been actually synthesized and their dielectric behavior has been examined.[45,46] In contrast, the hypothetical, partially dipole-labeled PI cannot be synthesized. $\Phi_{part}(t)$ for this hypothetical PI can be evaluated if the eigenfunctions f_p and eigenvalues $1/\tau_p$ are known for all relaxation modes.

dx.doi.org/10.1021/ma102595f |*Macromolecules* 2011, 44, 1585–1602

However, f_p and $1/\tau_p$ have been dielectrically determined only for the lowest three modes,[45,46] and we cannot accurately evaluate $\Phi_{part}(t)$ for general cases. Nevertheless, for a special case that the hypothetical PI chain is dipole-labeled in *half* of its backbone, eqs 11−13 allow us to simply express $\Phi_{half\text{-}label}(t)$, without any detailed knowledge for f_p and $1/\tau_p$, as

$$\Phi_{half\text{-}label}(t) = \frac{1}{2}\{\Phi_{ord}(t) + \Phi_{sym\text{-}inv}(t)\} \qquad (14)$$

Here, $\Phi_{ord}(t)$ and $\Phi_{sym\text{-}inv}(t)$ are the dielectric relaxation functions for the ordinary and symmetrically dipole-inverted linear PI chains having the same molecular weight M and exhibiting the same motion as the *half-label* PI chain of our interest. The dielectric behavior has been examined for such a pair of the ordinary and dipole-inverted PI49 with $M = 48.8 \times 10^3$ ($\cong 10M_e^{bulk}$), and the dielectric relaxation has been found to be $\cong$4 times faster for the latter (because of the dielectric inertness of odd eigenmodes for the latter).[45,46] Thus, and $\Phi_{sym\text{-}inv}(t)$ and $\Phi_{ord}(t)$ satisfy a relationship, $\Phi_{sym\text{-}inv}(t) = \Phi_{ord}(4t)$, and eq 14 is rewritten as

$$\Phi_{half\text{-}label}(t) = \frac{1}{2}\{\Phi_{ord}(t) + \Phi_{ord}(4t)\} \qquad (15)$$

In our PI53−PtBS42 copolymer, the PtBS42 block occupies 30% of the backbone measured in terms of the number of entanglement segments; see the θ value in eq 9b. This fraction is different from but fairly close to the fraction (50%) considered in eq 15. Thus, as the best approximation at this moment, we may compare, on the basis of eq 15, the $\varepsilon_{PI\ block}^*(\omega;T)$ data of the PI53−PtBS42 copolymer at T and $\{\varepsilon_{PI66}^*(\lambda'\omega;T_{iso\text{-}PI}^{bulk}) + \varepsilon_{PI66}^*(\lambda'\omega/4;T_{iso\text{-}PI}^{bulk})\}/2$ of the equivalent PI66 at $T_{iso\text{-}PI}^{bulk} = T - 30$ °C. Since the dielectric data are available for the ordinary and dipole-inverted PI49 samples[45] but not for PI66, the actual comparison is made for the $\varepsilon_{PI\ block}^*(\omega;T)$ data and the data obtained for the ordinary PI49 sample,

$$\varepsilon_{eqv}^*(\omega;T) \equiv \frac{\phi_{PI} b_T}{2}\{\varepsilon_{PI49}^*(r_\tau'\lambda'\omega;T_{iso\text{-}PI}^{bulk}) + \varepsilon_{PI49}^*(r_\tau'\lambda'\omega/4;T_{iso\text{-}PI}^{bulk})\} \qquad (16)$$

Here, the PI volume fraction ϕ_{PI} and the intensity factor $b_T = T_{iso\text{-}PI}^{bulk}/T$ are multiplied for correction of the dielectric intensity difference between the PI49 sample and the PI block (as done in eq 6). A minor correction factor r_τ' for the molecular weight difference between PI49 and the equivalent PI66 is evaluated as

$$r_\tau' = \left(\frac{M_{PI66}}{M_{PI49}}\right)^{3.5} = 2.9 \qquad (17)$$

The result of the above comparison is later shown in Figures 7 and 9.

4.3. Comparison of Dielectric Behavior of PI−PtBS Copolymer and Equivalent PI. *4.3.1. Comparison of τ_ε.* In Figure 7, the dielectric $\tau_\varepsilon(T)$ data of the PI53−PtBS42 copolymer at various T(circles)[54] are compared with $\tau_\varepsilon^{eqv}(T)$ of the equivalent star and linear PI obtained from $\varepsilon_{eqv}^*(\omega;T)$ defined by eqs 6 and 16. This $\varepsilon_{eqv}^*(\omega;T)$ was evaluated from the available data for the bulk PI$(59)_6$ and PI49 samples at $T_{iso\text{-}PI}^{bulk} = T - 30$ °C, as explained earlier. The τ_ε(T) data of the copolymer are close to $\tau_\varepsilon^{eqv}(T)$ of the equivalent star and linear PI at low and high T, respectively, and the crossover between these asymptotes is noted at intermediate T. This result lends support to the molecular picture that the PI53 block behaves as the equivalent star and linear chains at low and high T. Thus, the thermorheological complexity of the dielectric data for the copolymer at low ω (top panel of Figure 4) is mainly attributable to the crossover of the motional mode, as discussed earlier.

4.3.2. Comparison of Relaxation Mode Distribution at Lowest T (20 °C). Following eq 6, we utilized the dielectric $\varepsilon_{PI(59)6}^*(\omega;T_{iso\text{-}PI}^{bulk})$ data of the star PI$(59)_6$ sample[31] reduced at $T_{iso\text{-}PI}^{bulk} = -10$ °C (263 K) to evaluate $\varepsilon_{eqv}^*(\omega;T)$ for the equivalent star PI at $T = 20$ °C (293 K). In the top panel of Figure 8, the $\Delta\varepsilon_{eqv}'(\omega)$ and $\varepsilon_{eqv}''(\omega)$ of the equivalent star PI (solid curves) are compared with the $\Delta\varepsilon'(\omega)$ and $\varepsilon''(\omega)$ data of the PI53−PtBS42 copolymer at 20 °C. The filled triangles indicate plot of the $\Delta\varepsilon'(\omega)$ data of the PI53/PtBS42 reference blend with $w_{PI} = 55.7$ wt % at 20 °C (in the iso-τ_e state). For clear comparison, this plot is slightly shifted upward in the double logarithmic scale so that it agrees with the $\Delta\varepsilon'(\omega)$ plot for the copolymer (unfilled squares) at the highest ω in the panel. The bottom panel compares the modulus data of the PI53−PtBS42 copolymer (symbols) and the PI53/PtBS42 blend (curves) at 20 °C.

The copolymer chain has N_e =13.2 entanglements per chain, as explained earlier. The corresponding plateau modulus sustained by both PI and PtBS blocks is evaluated to be $G_N = \nu_{chain} N_e k_B T = 3.3 \times 10^5$ Pa (ν_{chain} = chain number density). In the bottom panel of Figure 8, we note that $G' > G_N$ at $\omega > 2\ s^{-1}$ and the Rouse-like power-law behavior $G' \cong G'' \propto \omega^{1/2}$ is observed in this high-ω zone. Thus, at $\omega > 2\ s^{-1}$, the PI and PtBS blocks appear to equilibrate themselves within the entanglement length a through the cooperative Rouse mechanism, as discussed for high-M blends.[35] Consequently, the entanglement relaxation occurs at $\omega < 2\ s^{-1}$. The dominant part of the dielectric relaxation of the PI block is observed in this low-ω zone (top panel), which is consistent with the molecular picture that that the PI53 block essentially behaves as a star arm at low T.

Now, we focus on the dielectric behavior shown in the top panel of Figure 8. We first note that the dielectric relaxation is significantly slower for the PI53 block of the copolymer (unfilled symbols) than for the PI53 chain in the blend (filled triangle). This result demonstrates that the PI block motion is strongly constrained by the PtBS block at 20 °C. Furthermore, the curves for the equivalent star PI are close to the $\Delta\varepsilon'(\omega)$ and $\varepsilon''(\omega)$ data of the copolymer. This result lends support to the above molecular picture.

At the same time, we should again emphasize that the PI and PtBS blocks do have the same, slowest eigenmode relaxation time and the PI block relaxation is much faster than the PtBS block relaxation in a sense that the intensity of the slowest eigenmodes is smaller for the PI block. Consequently, the *real slowest* relaxation process of the PI block should occur simultaneously with that process of the PtBS block and the PtBS block cannot be regarded as the fixed anchor for the PI block during this process.

In relation to this point, we note that G' of the copolymer decreases to the entanglement plateau modulus expected for the case of simple dilation of entanglement by the relaxed PI block, $G_N^{dil} = \phi_{PtBS}^{2.3} G_N = 4.3 \times 10^4$ Pa, with decreasing ω to $\omega_c = 0.06\ s^{-1}$; see the arrow in the bottom panel. This viscoelastic feature suggests that the PtBS block begins to exhibit rather significant motion/relaxation at such low $\omega \leq \omega_c$. The terminal part of the dielectric relaxation of the PI block does occur in this range of ω (cf. top panel), suggesting that the motion of the PtBS block affects (accelerates) the PI relaxation at those ω. Indeed, a hint of

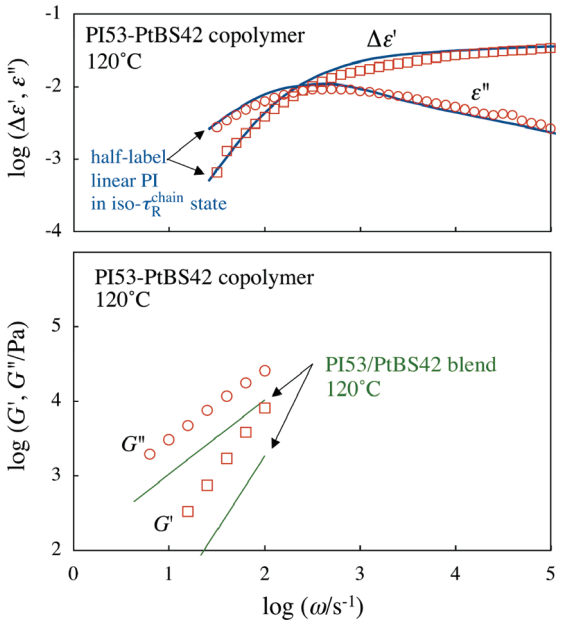

Figure 9. Top panel: Comparison of the dielectric $\Delta\varepsilon'$ and ε'' data for the PI53−PtBS42 copolymer at 120 °C (unfilled symbols) and the equivalent linear PI (M = 66.1 × 10^3; thick solid curves) having the entanglement number identical to that for the copolymer chain as a whole. The comparison is made in the iso-τ_R^{chain} state where the equivalent linear PI and the PI−PtBS copolymer have the same longest Rouse relaxation time. Bottom panel: Comparison of the viscoelastic G' and G'' data for the PI53−PtBS42 copolymer (unfilled symbols) and the PI53/PtBS42 blend (curves) at 120 °C.

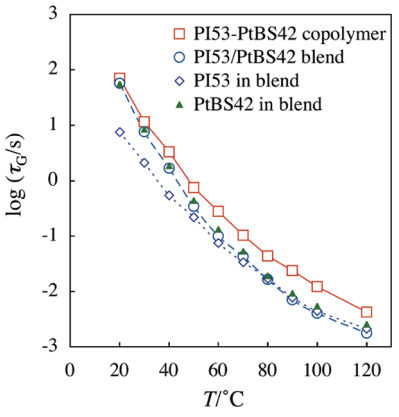

Figure 10. Comparison of the viscoelastic terminal relaxation time τ_G for the PI53−PtBS42 copolymer, the PI53/PtBS42 blend, and the PI53 and PtBS42 chains in the blend.

this acceleration can be noted as the downward deviation of the $\Delta\varepsilon'(\omega)$ data of the PI block from the equivalent PI curve at those ω. In addition, because of the block connectivity, the PtBS segment near the PI−PtBS junction would be more significantly plasticized by the PI segments compared to the other PtBS segments far from the junction. The junction point fluctuation due to this extra plasticization might enhance the difference between the PI block and star PI. Thus, the full relaxation behavior of the PI block at low T is close but not identical to that of the equivalent star PI. Accurate description of this behavior of the PI block requires a molecular analysis for a block anchored by a slow but mobile block. This analysis is an interesting subject of future work.

4.3.3. Comparison of Relaxation Mode Distribution at Highest T (120 °C). Following eq 16, we utilized the dielectric $\varepsilon_{PI49}^*(\omega;T_{iso\text{-}PI}^{bulk})$ data of the linear PI49 sample[45] reduced at $T_{iso\text{-}PI}^{bulk}$ = 90 °C to evaluate $\varepsilon_{eqv}^*(\omega;T)$ for the equivalent, half-labeled linear PI at T = 120 °C. The top panel of Figure 9 compares the $\Delta\varepsilon_{eqv}'(\omega)$ and $\varepsilon_{eqv}''(\omega)$ of this equivalent PI (solid curves) with the data of the PI53−PtBS42 copolymer at 120 °C (unfilled symbols). The bottom panel compares the modulus data of the PI53−PtBS42 copolymer (symbols) and the PI53/PtBS42 blend (curves) at 120 °C.

At low ω where the dominant part of the dielectric relaxation of the PI block is observed, G' of the copolymer is well below the entanglement plateau modulus sustained by both PI and PtBS blocks, $G_N = \nu_{chain}N_e k_B T$ = 4.4 × 10^5 Pa (at 120 °C); cf. bottom panel. This fact indicates that the entanglement segment of the size a (= 6.2 nm; cf. eq 3) behaves as the internally equilibrated motional unit for the dielectrically detected global relaxation process of the copolymer. Thus, the dielectric data of the equivalent linear PI, being evaluated with the entanglement segment as the motional unit (cf. eqs 9a and 10), can be unequivocally compared with the copolymer data.

As explained earlier, $\langle R^2\rangle$ is not exactly the same for the PI and PtBS blocks and no complete agreement is expected for the data of the copolymer and the equivalent linear PI, the latter having the dipoles in its *half* backbone. Nevertheless, the dielectric data of the equivalent PI agree with the copolymer data surprisingly well; see top panel. This result strongly suggests the basic validity of the molecular picture that the PI53 block at high T behaves as a portion of free linear chain (subjected to an extra friction from the PtBS block).

4.4. Dynamics of Copolymer Chain. For the PI53−PtBS42 copolymer, the PtBS block dynamics is also a subject of our interest. However, we cannot dielectrically examine the global motion of the PtBS block having no type-A dipole. Furthermore, for the *mutually connected* PI and PtBS blocks, we have no simple blending law for the viscoelastic moduli sustained by respective blocks. For this reason, this section focuses on the behavior of the PI−PtBS copolymer chain as a whole to discuss the relaxation of the PtBS block just qualitatively.

4.4.1. Viscoelastic Relaxation Time of the Copolymer. Figure 10 compares the terminal viscoelastic relaxation times τ_G of the PI53−PtBS42 copolymer (unfilled squares) and the PI53/PtBS42 blend (unfilled circles), both having the same PI content (w_{PI} = 55.7 wt %). In the copolymer and blend at the same T, the iso-τ_s state is achieved not only for the Rouse segment of PI but also for that of PtBS. The relaxation times of the PI53 and PtBS42 chains in the blend, evaluated from the analysis of the blend data (Appendix B), are also shown for comparison; cf. unfilled diamonds and filled triangles.

At low T, τ_G is similar for the copolymer, blend, and the PtBS42 chain in the blend but significantly smaller for the PI53 chain in the blend, which is in harmony with the earlier discussion for the PI block relaxation: Namely, at low T, the PtBS42 block is the "slow" block (defined by considering both relaxation time and intensity of eigenmodes) and thus behaves as the anchor during the dominant part of the PI block relaxation. Consequently, at the onset of the terminal relaxation of the copolymer (where the PI block has relaxed considerably), the connectivity with the PI53 block would not significantly affect the PtBS42 block motion. Then, τ_G of the PtBS42 block is expected to be close to τ_G of the copolymer and also to τ_G of the PtBS42 chain in the blend being free from the connectivity effect. This

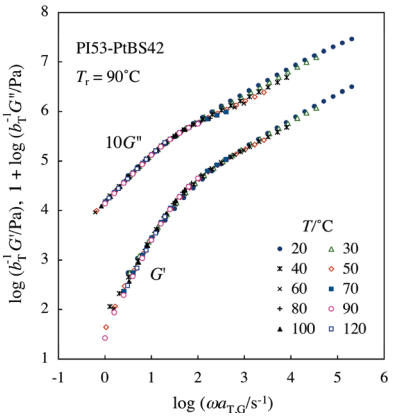

Figure 11. Test of time−temperature superposability for the viscoelastic G' and G'' data for the PI53−PtBS42 copolymer. The data are reduced by the intensity factor, $b_T = T/T_r$ (with T_r = 363 K), and superposed at their low-ω G'' tails. The G'' data are multiplied by a factor of 10 to avoid heavy overlapping with the G' data.

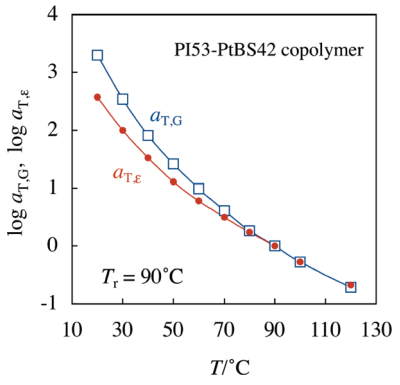

Figure 12. Comparison of the viscoelastic and dielectric shift factors $a_{T,G}$ and $a_{T,\varepsilon}$ for the PI53−PtBS42 copolymer utilized for the superposition in Figures 11 and 4.

expectation is in harmony with the low-T data in Figure 10. However, we should also note that the viscoelastic G^* data of the copolymer and blend at low ω are close but not identical to each other; see the bottom panel of Figure 8. This result suggests that the PI block has some effect on the relaxation of the copolymer/PtBS block possibly because the real slowest relaxation of the PI block occurs cooperatively with the PtBS42 block, as discussed earlier.

In contrast, at high T, τ_G of the copolymer is larger than τ_G's of the blend and the PI53 and PtBS42 chains therein; cf. Figure 10. Thus, the PtBS42 and PI53 blocks connected to each other appears to relax cooperatively thereby allowing the copolymer chain to behave as the equivalent linear chain that has a larger M and relaxes slower compared to the PI53 and PtBS42 chains in the blend. This effect of the block connectivity makes a significant contrast between the relaxation of the copolymer and blend at high T.

At intermediate T, τ_G of the copolymer exhibits a crossover between the two asymptotic cases discussed above. This crossover of τ_G, due to the crossover of the motional mode of the PI block and the corresponding change in the PtBS block motion, cannot be described by the molecular models available at this moment. Formulation of a model describing this crossover behavior is an interesting subject for future work.

4.4.2. Thermo-Rheological Behavior of the Copolymer. In Figure 11, the storage and loss moduli, G' and G'', measured for the copolymer at various T are reduced by an intensity correction factor, $b_T = T/T_r$ (T and T_r in K unit), and shifted along ω axis by a factor of $a_{T,G}$ to achieve the best superposition of their low-ω G'' tails. The reference temperature is chosen to be T_r = 363 K (90 °C). The G'' data are multiplied by a factor of 10 in order to avoid heavy overlapping with the G' data. In Figure 12, the viscoelastic shift factor $a_{T,G}$ utilized for this superposition is compared with the dielectric shift factor $a_{T,\varepsilon}$ achieving the superposition of the $\Delta\varepsilon'$ and ε'' data of the copolymer (cf. top panel of Figure 4.)

As noted in Figure 11, a fairly good superposition is achieved for the G^* data of the copolymer. However, a close inspection reveals a failure of superposition at intermediate to high ω; see the data at $\omega a_{T,G}$/s^{-1} = 10^2 − 10^5. This delicate failure possibly reflects the change of the motional mode of the PI block with T (from the tethered chain like motion at low T to the free chain like motion at high T retarded by the PtBS block) and the corresponding change for the PtBS block motion. The copolymer chain should be thermorheologically complex because of these changes of the motional modes. However, this viscoelastic complexity is much less significant compared to the dielectric complexity (cf. top panel of Figure 4), as also noted for miscible PI−PVE block copolymers.[9]

This difference of the viscoelastic and dielectric complexities of the PI−PtBS copolymer can be related to a fact that the dielectric data just detect the global motion of the PI block while the viscoelastic data are contributed from both of the PI and PtBS blocks. As the motional mode of the PI block changes with increasing T, the PI contribution to the terminal relaxation of the copolymer is enhanced while that to the fast relaxation becomes less significant. Correspondingly, the PtBS contributions to the slow and fast parts of the copolymer relaxation become less and more significant with increasing T. These changes of the PI and PtBS contributions tend to cancel each other, which possibly resulted in the weak viscoelastic complexity seen in Figure 11.

The viscoelastic shift factor $a_{T,G}$ of the copolymer is evaluated from the low-ω moduli data. Thus, we expect that $a_{T,G}$ of the copolymer at low T reflects the motion of the PtBS block (much slower than the motion of the PI block) while that at high T corresponds to the cooperative motion of the PI and PtBS blocks. This expectation is in harmony with the observation in Figure 12 that $a_{T,G}$ at low T is larger and more strongly dependent on T compared to $a_{T,\varepsilon}$ reflecting the PI block motion while $a_{T,G}$ at high T is very similar, in the T dependence as well as the magnitude, to the dielectric $a_{T,\varepsilon}$. This result again lends support to the molecular picture that the PI block essentially behaves as the tethered chain at low T while as a portion of the free linear chain at high T.

5. CONCLUDING REMARKS

Linear viscoelastic and dielectric behavior was examined for a disordered PI53−PtBS42 diblock copolymer and the PI53/PtBS42 reference blend having the same PI content (w_{PI} = 55.7 wt %). For these samples, the dielectric data characterize the global motion of PI block/chain, while the viscoelastic data detect the relaxation of all components in the blend/copolymer systems.

Comparison of the dielectric and viscoelastic terminal relaxation times suggested that the relaxation of the PI and PtBS blocks of the copolymer is affected by the antiplasticization and plasticization due to respective partner blocks, as similar to the situation in the PI/PtBS blends. However, more importantly, the block relaxation was found to be strongly affected by the connectivity between the blocks. This connectivity effect, being absent in the blends, forced the PI block

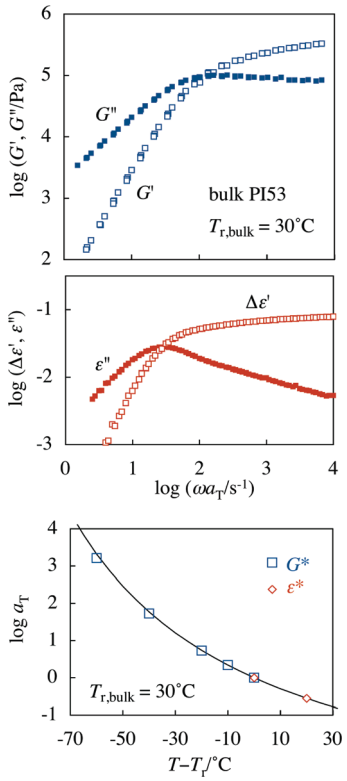

Figure 13. Viscoelastic G' and G'' data (top panel) and dielectric $\Delta\varepsilon'$ and ε'' data (middle panel) of bulk PI53 reduced at T_r = 30 °C. The plots in the bottom panel show the shift factors for these data, and the solid curve indicates the WLF equation for bulk PI (eq A1).

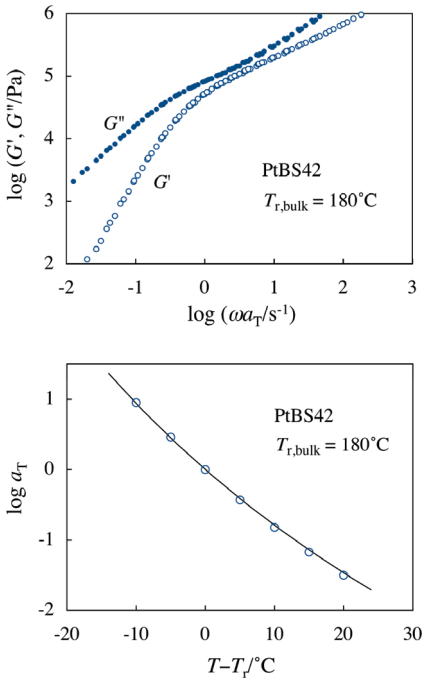

Figure 14. Viscoelastic G' and G'' data of bulk PtBS42 reduced at T_r = 180 °C (top panel) and the shift factor for these data (bottom panel). The solid curve in the bottom panel indicates the WLF equation for bulk PtBS (eq A2).

to relax essentially as the tethered chain (anchored by the slow PtBS block) at low T while as a portion of free linear chain at high T (where the PI and PtBS blocks relax cooperatively). This change of the motional mode of the PI block with T led to the thermorheological complexity of the dielectric data that was much more significant compared to the complexity of the PI/PtBS reference blend. The corresponding complexity was observed also for the viscoelastic data of the copolymer. However, this viscoelastic complexity was much less prominent than the dielectric complexity, possibly because viscoelastic changes due to the mode changes of the PI and PtBS blocks tend to cancel each other.

Finally, we note that the connectivity effect on the global dynamics of the disordered PI−PtBS diblock copolymers would change with the entanglement density. Specifically, for nonentangled copolymers, the reduction of the frictional asymmetry between the PI and PtBS blocks on the increase of T is expected to result in the crossover from the tethered Rouse-like behavior of the PI block to the nontethered Stockmayer-Kennedy type behavior of the copolymer as a whole. It is an interesting subject of future work to test this expectation for low-M PI−PtBS copolymers.

■ APPENDIX A. DYNAMIC BEHAVIOR OF BULK COMPONENTS

For bulk PI53 sample, the time−temperature superposition held well for the viscoelastic $G'(\omega)$and $G''(\omega)$ data as well as for the dielectric $\Delta\varepsilon'(\omega)$ $(=\varepsilon'(0) - \varepsilon'(\omega))$ and $\varepsilon''(\omega)$ data. The master curves of these data, reduced at a bulk reference temperature $T_{r,bulk}$ = 30 °C, are shown in the top and middle panels of Figure 13. The dielectric and viscoelastic shift factors a_T coincide with each other (because the slow viscoelastic and dielectric relaxation processes of PI detect the same global motion) and are commonly described by the previously reported WLF function[26] (cf. bottom panel of Figure 13).

$$\log a_T = -\frac{4.425(T - T_{r,\,bulk})}{140.0 + T - T_{r,\,bulk}} \quad \text{with } T_{r,\,bulk} = 30\ ^\circ\text{C} \tag{A1}$$

The PtBS42 chains have no type-A dipole and thus their global motion is dielectrically inert.[35] However, this motion is unequivocally reflected in the $G'(\omega)$ and $G''(\omega)$ data. These data obeyed the time−temperature superposition, and their master curves at $T_{r,bulk}$ = 180 °C are shown in top panel of Figure 14. The corresponding shift factor a_T is well described by the WLF equation reported previously,[25] as shown in the bottom panel of Figure 14.

$$\log a_T = -\frac{10.0(T - T_{r,\,bulk})}{116.5 + T - T_{r,\,bulk}} \quad \text{with } T_{r,\,bulk} = 180\ ^\circ\text{C} \tag{A2}$$

■ APPENDIX B. ISO-T_S STATE FOR COMPONENTS IN BLENDS AND COPOLYMER

B1. Iso-τ_s State for PI. The top panel of Figure 5 shows the shift factor $a_{T,\varepsilon}$ utilized for the superposition of the dielectric data of the PI53−PtBS42 copolymer and the PI53/PtBS42 blend at high $\omega \geq \omega_{peak}$ (cf. Figure 4). The $a_{T,\varepsilon}$ data defined with respect to T_r = 90°C are almost indistinguishable for these systems having the same w_{PI} (=55.7 wt %), suggesting a similarity of the local frictional

environment for the Rouse segment (smallest motional unit for the rubbery relaxation) of the PI chain/block therein.

For the PI/PtBS blend, $a_{T,\varepsilon}$ is determined by two mechanisms affecting the PI relaxation, the anti-plasticization of PI due to PtBS and the change of the contribution of the dynamic tube dilation (DTD)/constrain release (CR) mechanism to the PI relaxation on blending with PtBS.[26] The latter change is minor in a quantitative sense.[26] However, in this study, we correct the $a_{T,\varepsilon}$ data for the second mechanism because of its conceptual importance.

The change of the DTD/CR contribution to the PI relaxation on blending with PtBS can be quantified by a Q factor being introduced as a ratio of the dielectric τ_ε of the fast component in PI/PI blends to τ_ε of this component in bulk state.[26] For our PI53/PtBS42 blend, the Q factor was evaluated from eq 9 of ref 26, with the numerical coefficients therein being given by (B, α, q) = (0.35, 0.2, 2.5) for $\phi_{PtBS} = 0.41$ (= ϕ_2 in eq 9 of ref 26). The raw data of the shift factor $a_{T,\varepsilon}$ were corrected for the change of the DTD/CR contribution as $a_{T,\varepsilon}^* = a_{T,\varepsilon}/Q$, with $1 \le Q \le 1.14$ for our PI/PtBS blend at $T \ge 20$°C. (Thus, in a quantitative sense, this correction represented by the Q factor was minor.) This $a_{T,\varepsilon}^*$ represents exclusively the change of relaxation time τ_s of the Rouse segment of PI in the blend with T.

The standard WLF analysis[26] for the $a_{T,\varepsilon}^*$ data of the PI/PtBS blends gave the iso-τ_s temperature for the blends, $T_{iso\text{-}PI} = 60$°C, that corresponds to the reference temperature of bulk PI, $T_{r,bulk} = 30$°C. For the PI53/PtBS42 blend as well as the other PI/PtBS blends having the same w_{PI} (=55.7 wt %) examined elsewhere,[51] the bottom panel of Figure 5 shows the plots of $a_{T,iso}$ (=$a_{T,\varepsilon}^*$ defined with respect to $T_{iso\text{-}PI}$) against $T - T_{iso}$. (The sample code number indicates $10^{-3}M$.) The plots are excellently described by the WLF equation for bulk PI (curve), eq A1 with $T_{r,bulk} = T_{iso\text{-}PI}$, indicating the reliability of our WLF analysis. Thus, the Rouse segment of PI in the blends at T is in the iso-τ_s state with respect to the segment in PI bulk at $T' = T - \Delta T_{iso-PI}$ (=$T - 30$). This should be the case also for the PI segment of the PI–PtBS copolymer having the same w_{PI} (=55.7 wt %) as the PI/PtBS blends.

B2. Iso-τ_s State for PtBS. For determination of the iso-τ_s temperature for the Rouse segment of PtBS, we first need to evaluate the modulus G_{PtBS}^* of the PtBS chain in the PI/PtBS blends and then make the WLF analysis for the shift factor a_T for the modulus data. In the PI53/PtBS42 blend, the PtBS42 relaxation is slower/equally slow compared to the PI53 relaxation in the entire range of T examined, as explained for Figure 3. Thus, the PtBS modulus in the blend can be evaluated from the $G_B^*(\omega,T)$ data of the blend and the $G_{PI,bulk}^*(\omega,T_{r,bulk})$ data of bulk PI53 at its reference temperature $T_{r,bulk}$ (=303 K) with the aid of a blending law explained in our previous work,[25,26,35]

$$G_{PtBS}^*(\omega;T) = G_B^*(\omega;T) - \frac{\phi_{PI} I_e}{b_T'} G_{PI,bulk}^*(\omega Q^{2.33}/\lambda_{PI};T_{r,bulk}) \quad \text{(B1)}$$

Here, b_T' (= $T_{r,bulk}/T$) gives the intensity correction between temperatures T and $T_{r,bulk}$, I_e (= $\{a_{PI}^{bulk}/a\}^2$ = 0.88; cf. eq 3) represents the decrease of the entanglement plateau modulus G_N on blending of PI and PtBS, ϕ_{PI} (= 0.59) is the PI volume fraction in the blend, Q is a factor specifying an increase of τ_ε of PI in the blend due to restriction of DTD/CR, and λ_{PI} is a ratio of the dielectric relaxation time of bulk PI53 at $T_{r,bulk}$ to that of PI53 in the blend at T. In eq B1, we have neglected a contribution of the minority PI53 in the PI53/PtBS42 blend to the PI modulus because the minority is rather dilute in the blend (as noted from just a weak thermo-rheological complexity of the ε'' data of the blend; cf. Figure 4). The correction for G_N through the factor I_e is minor in a numerical sense and was neglected in the previous work.[26] However, this correction has been incorporated in eq B1 for conceptual completeness.

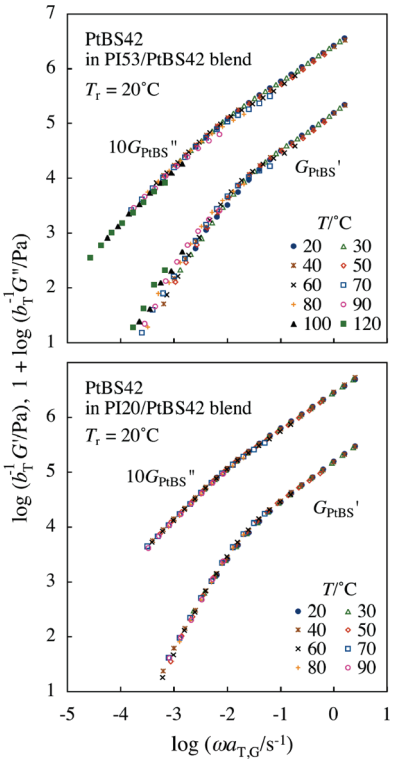

Figure 15. Test of the time–temperature superposability for the viscoelastic modulus data of the PtBS42 chain in the PI53/PtBS42 blend (top panel) and in the PI20/PtBS42 blend[51] (bottom panel). The reference temperature is T_r = 20 °C. The data are reduced by the intensity factor, $b_T = T/T_r$ (with T_r = 293 K), and superposed by utilizing the low-ω G_{PtBS}'' data as a guide. The G'' data are multiplied by a factor of 10 to avoid heavy overlapping with the G' data. For further details, see text.

The Q factor appearing in eq B1 was determined from the τ_G/τ_ε ratios measured for the blend and bulk PI53, as explained previously.[26] The λ_{PI} value was directly obtained from the ε'' peak frequencies for the blend at T and bulk PI53 at $T_{r,bulk}$. (The τ_ε data of the blend, being evaluated from the low-ω tails of the $\Delta\varepsilon'$ and ε'' data (cf. eq 1), were affected by the minority PI53. For this reason, we utilized the ω_{peak} data to evaluate λ_{PI}.) Thus, all parameters appearing in eq B1 were experimentally obtained, which enabled us to evaluate $G_{PtBS}^*(\omega,T)$ of PtBS42 in the PI53/PtBS42 blend. The viscoelastic relaxation time τ_G of PtBS42 in the blend was evaluated from those G_{PtBS}^* data obtained with the aid of eq B1 (that is valid in a range of ω where the entanglement segment is internally equilibrated and G' does not exceed the entanglement plateau modulus[35]). τ_G of PI53 in the blend was evaluated from the $\{\phi_{PI}I_e/b_T'\}G_{PI,bulk}^*(\omega Q^{2.33}/\lambda_{PI};T_{r,bulk})$ data utilized in eq B1. These τ_G data are shown in Figure 10.

We tested the time-temperature superposability of the PtBS modulus data obtained above by utilizing the low-ω G_{PtBS}'' data as a guide for the superposition. The results are shown in the top panel of Figure 15, where $G_{PtBS}^*(\omega,T)$ at respective T is reduced by the intensity factor $b_T = T/T_r$ (with T_r = 293 K) and plotted

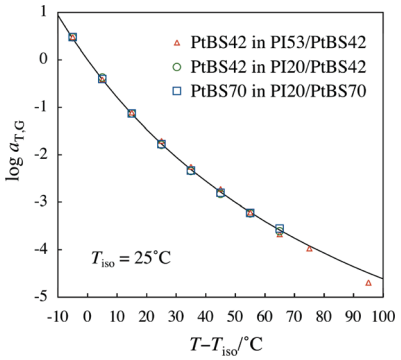

Figure 16. Shift factor $a_{T,G}$ utilized for the PtBS42 modulus in the PI53/PtBS42 and PI20/PtBS42 blends (examined in Figure 15) and for the PtBS70 modulus in the PI20/PtBS70 blend.[51] All these blends have the same composition, w_{PI} = 55.7 wt %. (For the PI20/PtBS42 and PI20/PtBS70 blends examined previously,[51] the viscoelastic response was dominated by PtBS chains and $a_{T,G}$ agreed with the shift factor for the modulus of the blend as a whole.) The solid curve indicates the WLF equation (eq A2) for PtBS with respect to the iso-τ_s temperature, $T_{iso\text{-}PtBS}$ = 25 °C for PtBS in the blends and $T_{r,bulk}$ = 180 °C for bulk PtBS42. For further details, see Appendix B.

against a reduced frequency $\omega a_{T,G}$. The superposition fails moderately, possibly because of a change of the motional mode of the PtBS42 chain with T: PtBS42 relaxes much more slowly compared to PI53 at low T, but this difference of the relaxation rates decreases with increasing T to enhance the topological effect of PI53 on the PtBS relaxation and induce this change of the motional mode. (This situation is qualitatively similar to that for the moderate thermo-rheological complexity of the G^* data of the PI−PtBS copolymer; cf. Figure 11).

From this mechanism of the complexity of the PtBS42 modulus, we naturally expect that the $G_{PtBS}^*(\omega,T)$ data obey the time-temperature superposition in a range of T where the PI motion is sufficiently faster than the PtBS42 motion. In fact, this situation is realized in a wide range of T if the PtBS42 chain is blended with lower-M (faster) PI. As an example, the bottom panel of Figure 15 demonstrates good superposability of the G_{PtBS}^* data recently obtained for the PtBS42 chain blended with lower-M PI20 chain ($M = 19._9 \times 10^3$) at the same w_{PI} (=55.7 wt %).[51] (Even more excellent superposition was achieved for the relaxation modulus $G_{PtBS}(t)$ of the PtBS chain because a relative contribution from the fast Rouse equilibration mode to $G_{PtBS}(t)$, if any, exponentially decays with t and vanishes in the terminal relaxation regime of our interest.[51]) Since PI20 relaxed much faster than PtBS42 in the range of T, those G_{PtBS}^* data obtained with the aid of eq B1 were almost indistinguishable from the raw G^* data of the blend and exhibited excellent superposition.[51] This was the case also for the previously examined low-M PI/PtBS blends.[25,26]

The excellent superposition seen for the PI20/PtBS42 blend indicates that the motional mode of the PtBS42 chain therein hardly changes with T. Standard WLF analysis of the shift factor $a_{T,G}$ for those data gave the iso-τ_s temperature for the Rouse segment of PtBS in the blend, $T_{iso\text{-}PtBS}$ = 25°C that corresponded to the reference temperature of bulk PtBS, $T_{r,bulk}$ = 180°C.[51] For the other PI20/PtBS70 blend ($M_{PtBS} = 69._{5\times10}{}^3$) with the same w_{PI} (= 55.7 wt %) exhibiting equally good superposition, the analysis again gave $T_{iso\text{-}PtBS}$ = 25°C.[51] In Figure 16, the $a_{T,G}$ data for these blends defined with respect to this $T_{iso\text{-}PtBS}$ is plotted against $T - T_{iso\text{-}PtBS}$ (cf. large circle and square).[51] The plots are excellently described by the WLF equation for bulk PtBS (eq A2) with $T_{r,bulk} = T_{iso\text{-}PtBS}$ = 180 °C (solid curve), indicating the reliability of the WLF analysis. (For the PtBS42 chain in the PI53/PtBS42 blend, the superposition failed moderately; cf. top panel of Figure 15. Nevertheless, its $a_{T,G}$ factor was rather close to the WLF description, as shown with the small triangle in Figure 16. For this blend, the approximate superposition utilizing the low-ω G_{PtBS}'' data as a guide may have reflected the correct $T_{iso\text{-}PtBS}$ with a rather small uncertainty.)

Since the friction coefficient of the Rouse segment is determined locally by the composition, the $T_{iso\text{-}PtBS}$ value obtained above should be common for the PI/PtBS blends and PI53−PtBS42 copolymer having the same w_{PI} (= 55.7 wt %). Thus, the Rouse segments of PtBS in the blends and copolymer at T are in the iso-τ_s state with respect to the segment in PtBS bulk at $T'' = T - \Delta T_{iso-PtBS} = T + 155$.

We also note that the corresponding, effective T_g of the Rouse segments in the blends/copolymer, $T_{g,PtBS}^{eff} = T_{g,PtBS}^{bulk} + \Delta T_{iso-PtBS} = -8$°C, is located at the high-T edge of the broad glass transition of the blend/copolymer, as shown with the thick dotted arrows in Figure 1. This behavior can be related to the difference between the Rouse segment and the monomeric segment, the latter being responsible for the thermally observed transition, as explained for Figure 1.

APPENDIX C. TERMINAL RELAXATION TIMES OF BULK PI AND BULK PTBS

The PI53 block of the PI53−PtBS42 copolymer is expected to essentially behave as the arm of star chain at low T and as a portion of a free, nontethered linear chain at high T, as discussed in the text. A test of this molecular picture requires us to evaluate the relaxation time of these equivalent star/linear PI chains. Literature data[31] enabling this evaluation are summarized below.

C1. Dielectric Relaxation Time of PI. The data for the terminal dielectric relaxation time, τ_ε defined by eq 1, are available for a series of entangled 6-arm star PI and linear PI in bulk state at 40°C.[31] These τ_ε data were reduced to 30°C with the aid of the WLF equation for bulk PI (eq A1) and plotted against the span molecular weight $2M_{arm}$ (for star PI) and/or the total molecular weight M (for linear PI) in Figure 17. (The WLF shift is identical for the star and linear PI.[31]) The plots in the range of M, $2M_{arm} > 50 \times 10^3$ (well entangled regime) are described by empirical equations shown with the curves:

$$\tau_\varepsilon/\mathrm{s} = 2.0 \times 10^{-10} M_{arm}{}^{1.5} \times \exp\{1.4 \times 10^{-4} M_{arm}\} \quad \text{for star PI at 30 °C} \qquad (C1)$$

$$\tau_\varepsilon/\mathrm{s} = 7.9 \times 10^{-19} M^{3.5} \quad \text{for linear PI at 30 °C} \qquad (C2)$$

These equations are utilized to evaluate τ_ε of the equivalent star and linear PI in the iso-τ_e and iso-τ_R^{chain} states, respectively, as explained in the text.

C2. Viscoelastic Relaxation Times of PI and PtBS. We can utilize the data for the terminal viscoelastic relaxation time τ_G^{bulk} (defined by eq 1) of monodisperse bulk PI and PtBS to evaluate the ratio of the friction coefficients of the entanglement segments of the PtBS and PI blocks at a given T, $L = \zeta_e^{PtBS\ block}(T)/\zeta_e^{PI\ block}(T)$. As an example, the top panel of Figure 18 shows the τ_G^{bulk} data for bulk PI[29−31] at $T_{iso\text{-}PI}^{bulk}$ = 90°C and bulk PtBS[55] at $T_{iso\text{-}PtBS}^{bulk}$ = 275°C plotted against the M/M_e^{bulk} ratio (unfilled symbols). These

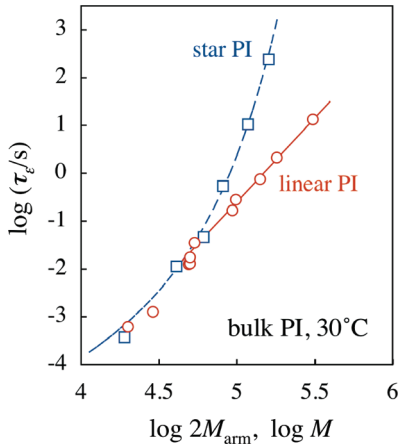

Figure 17. Plots of the dielectric relaxation time data[31] for 6-arm star PI (squares) and linear PI (circles) at 30 °C against the span molecular weight $2M_{arm}$ (for star PI) and total molecular weight M (for linear PI). The dashed curve and solid line, respectively, indicate empirical equations for star and linear PI (eqs C1 and C2) in the well-entangled regime (M, $2M_{arm} > 50 \times 10^3$).

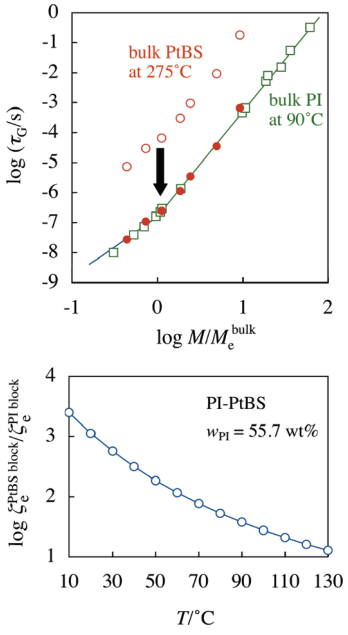

Figure 18. Top panel: Comparison of viscoelastic τ_G for bulk PI[29−31] at 90 °C (unfilled squares) and bulk PtBS[55] at 275 °C (unfilled circles). These temperatures are the iso-τ_s temperatures for the Rouse segments of PI and PtBS in the PI/PtBS blend (and copolymer) at T = 120 °C. The filled circles indicate the τ_G data for bulk PtBS multiplied by a factor of 3.7×10^{-3}. Bottom panel: A ratio of the friction coefficients of the entanglement segments of the PtBS and PI blocks, $\zeta_e^{PtBS\ block}(T)/\zeta_e^{PI\ block}(T)$, evaluated from the τ_G data of bulk PI and PtBS. This ratio is plotted against T. For further details, see Appendix C.

$T_{iso\text{-}PI}^{bulk}$ and $T_{iso\text{-}PtBS}^{bulk}$ are the iso-τ_s temperatures defined with respect to the Rouse segments of the PI and PtBS blocks at T = 120°C.

The filled circles in the top panel of Figure 18 indicate the $\tau_G^{bulk\ PtBS}(T_{iso\text{-}PtBS}^{bulk})$ data multiplied by 3.7×10^{-3}. As noted from the coincidence of those circles and squares ($= \tau_G^{bulk\ PI}(T_{iso\text{-}PI}^{bulk})$), the τ_G data of bulk PI and PtBS exhibit very similar M dependence, $\tau_G \propto M^2$ for $M/M_e^{bulk} < 1$ (unentangled behavior) and $\tau_G \propto M^{3.5}$ for $M/M_e^{bulk} > 1$ (entangled behavior). However, the magnitude of τ_G is different for the bulk PI and PtBS having the same M/M_e^{bulk} value, which essentially reflects the difference of $\zeta_e^{bulk\ PI}(T_{iso\text{-}PI}^{bulk})$ and $\zeta_e^{bulk\ PtBS}(T_{iso\text{-}PtBS}^{bulk})$. This difference of τ_G can be utilized to evaluate the $\zeta_e^{PtBS\ block}(T)/\zeta_e^{PI\ block}(T)$ ratio for the PtBS and PI blocks of the copolymer at T, as explained below.

The τ_G data of unentangled bulk PI and PtBS at T can be expressed in the Rouse form

$$\tau_G = \left[\frac{G'}{\omega G''}\right]_{\omega\to 0} = \frac{\{a_X^{bulk}\}^2 \zeta_e^{bulk\ X}(T)}{90 k_B T}\left(\frac{M}{M_e^{bulk\ X}}\right)^2 \quad (X = PI, PtBS) \tag{C3}$$

where $\zeta_e^{bulk\ X}(T)$ ($\propto N_R^{bulk\ X} \propto \{a_X^{bulk}\}^2$) is the friction coefficient of the entanglement segment of the size a_X^{bulk} in the bulk X system at T. (Considering the relationships for the chain friction coefficient $\zeta^{chain} = \zeta_e^{bulk\ X} M/M_e^{bulk}$ and for the chain size $\langle R^2\rangle = \{a_X^{bulk}\}^2 M/M_e^{bulk}$, we can rewrite the usual Rouse expression of τ_G into the form of eq C3.) Thus, for the bulk PI and PtBS having the *same* M/M_e^{bulk} ratio, eq C3 gives

$$\frac{\tau_G^{bulk\ PtBS}(T_{iso\text{-}PtBS}^{bulk})}{\tau_G^{bulk\ PI}(T_{iso\text{-}PI}^{bulk})} = \frac{T_{iso\text{-}PI}^{bulk}\{a_{PtBS}^{bulk}\}^2}{T_{iso\text{-}PtBS}^{bulk}\{a_{PI}^{bulk}\}^2}\frac{\zeta_e^{bulk\ PtBS}(T_{iso\text{-}PtBS}^{bulk})}{\zeta_e^{bulk\ PI}(T_{iso\text{-}PI}^{bulk})} = \frac{\{a_{PtBS}^{bulk}\}^4}{\{a_{PI}^{bulk}\}^4}\frac{\zeta_e^{PtBS\ block}(T)}{\zeta_e^{PI\ block}(T)} \tag{C4}$$

In derivation of eq C4, we have considered the following iso-τ_s relationship for the X block and bulk X (cf. eq 4):

$$\frac{\zeta_e^{bulk\ X}(T_{iso\text{-}X}^{bulk})}{T_{iso\text{-}X}^{bulk}} = \frac{\zeta_s^{bulk\ X}(T_{iso\text{-}X}^{bulk})}{T_{iso\text{-}X}^{bulk}} N_R^{bulk\ X} = \frac{\zeta_s^{X\ block}(T)}{T} N_R^{bulk\ X} = \frac{N_R^{X\ block}\zeta_s^{X\ block}(T)}{T}\left(\frac{N_R^{bulk\ X}}{N_R^{X\ block}}\right) = \frac{\zeta_e^{X\ block}(T)}{T}\left(\frac{a_X^{bulk}}{a}\right)^2 \tag{C5}$$

Equation C4 allows us to evaluate the $\zeta_e^{PtBS\ block}(T)/\zeta_e^{PI\ block}(T)$ ratio for the entanglement segments of the PtBS and PI blocks from the data for the $\tau_G^{bulk\ PtBS}(T_{iso\text{-}PtBS}^{bulk})/\tau_G^{bulk\ PI}(T_{iso\text{-}PI}^{bulk})$ and $a_{PtBS}^{bulk}/a_{PI}^{bulk}$ ratios: For example, the data in the top panel of Figure 18 give $\zeta_e^{PtBS\ block}(T)/\zeta_e^{PI\ block}(T) = 16.3$ at T = 120 °C. The bottom panel shows plots of the $\zeta_e^{PtBS\ block}(T)/\zeta_e^{PI\ block}(T)$ ratio thus obtained. This ratio changes with T according to the WLF feature of $\tau_G^{bulk\ X}$ (X = PI, PtBS) described by the eqs A1 and A2. The iso-τ_R^{chain} state of the PI−PtBS copolymer is specified with the aid of the $\zeta_e^{PtBS\ block}/\zeta_e^{PI\ block}$ ratio, as explained for eqs 8−10 in the text.

AUTHOR INFORMATION

Corresponding Author

*E-mail: hiroshi@scl.kyoto-u.ac.jp.

■ ACKNOWLEDGMENT

This work was partly supported by a Grant-in-Aid for Scientific Research on Priority Area "Soft Matter Physics" from the Ministry of Education, Culture, Sports, Science and Technology (Grant No. 18068009) and Grant-in-Aid for Young Scientists (B) from MEXT Grant No. 22750204). Q.C. expresses thanks for support from JSPS.

■ REFERENCES

(1) Lodge, T. P.; McLeish, T. C. B. *Macromolecules* **2000**, *33*, 5278–5284.
(2) Chung, G. C.; Kornfield, J. A.; Smith, S. D. *Macromolecules* **1994**, *27*, 964–973.
(3) Alegria, A.; Colmenero, J.; Ngai, K. L.; Roland, C. M. *Macromolecules* **1994**, *27*, 4486–4492.
(4) Kumar, S. K.; Colby, R. H.; Anastasiadis, S. H.; Fytas, G. *J. Chem. Phys.* **1996**, *105*, 3777–3788.
(5) Wetton, R. E.; Macknight, W. J.; Fried, J. R.; Karasz, F. E. *Macromolecules* **1978**, *11*, 158–165.
(6) Liang, K. M.; Banhegyi, G.; Karasz, F. E.; Macknight, W. J. *J. Polym. Sci., B: Polym. Phys.* **1991**, *29*, 649–657.
(7) Miura, N.; MacKnight, W. J.; Matsuoka, S.; Karasz, F. E. *Polymer* **2001**, *42*, 6129–6140.
(8) Arendt, B. H.; Krishnamoorti, R.; Kannan, R. M.; Seitz, K.; Kornfield, J. A.; Roovers, J. *Macromolecules* **1997**, *30*, 1138–1145.
(9) Hirose, Y.; Urakawa, O.; Adachi, K. *J. Polym. Sci., B: Polym. Phys.* **2004**, *42*, 4084–4094.
(10) Roovers, J.; Toporowski, P. M. *Macromolecules* **1992**, *25*, 3454–3461.
(11) Roovers, J.; Wang, F. *J. Non-Cryst. Solids* **1994**, *172*, 698–704.
(12) Kanetakis, J.; Fytas, G.; Kremer, F.; Pakula, T. *Macromolecules* **1992**, *25*, 3484–3491.
(13) Chung, G. C.; Kornfield, J. A.; Smith, S. D. *Macromolecules* **1994**, *27*, 5729–5741.
(14) He, Y. Y.; Lutz, T. R.; Ediger, M. D. *Macromolecules* **2003**, *36*, 8040–8048.
(15) He, Y. Y.; Lutz, T. R.; Ediger, M. D.; Lodge, T. P. *Macromolecules* **2003**, *36*, 9170–9175.
(16) Haley, J. C.; Lodge, T. P.; He, Y. Y.; Ediger, M. D.; von Meerwall, E. D.; Mijovic, J. *Macromolecules* **2003**, *36*, 6142–6151.
(17) He, Y. Y.; Lutz, T. R.; Ediger, M. D. *Macromolecules* **2004**, *37*, 9889–9898.
(18) Hirose, Y.; Urakawa, O.; Adachi, K. *Macromolecules* **2003**, *36*, 3699–3708.
(19) Urakawa, O. *Nihon Reoroji Gakkaishi (J. Soc. Rheol. Jpn.)* **2004**, *32*, 265–270.
(20) Yao, M. L.; Watanabe, H.; Adachi, K.; Kotaka, T. *Macromolecules* **1991**, *24*, 2955–2962.
(21) Stühn, B.; Stickel, F. *Macromolecules* **1992**, *25*, 5306–5312.
(22) Floudas, G.; Paraskeva, S.; Hadjichristidis, N.; Fytas, G.; Chu, B.; Semenov, A. *J. Chem. Phys.* **1997**, *107*, 5502–5509.
(23) Watanabe, H. *Macromol. Rapid Commun.* **2001**, *22*, 127–175.
(24) Yurekli, K.; Krishnamoorti, R. *J. Polym. Sci., B: Polym. Phys.* **2004**, *42*, 3204–3217.
(25) Watanabe, H.; Matsumiya, Y.; Takada, J.; Sasaki, H.; Matsushima, Y.; Kuriyama, A.; Inoue, T.; Ahn, K. H.; Yu, W.; Krishnamoorti, R. *Macromolecules* **2007**, *40*, 5389–5399.
(26) Chen, Q.; Matsumiya, Y.; Masubuchi, Y.; Watanabe, H.; Inoue, T. *Macromolecules* **2008**, *41*, 8694–8711.
(27) Zhao, J. S.; Ediger, M. D.; Sun, Y.; Yu, L. *Macromolecules* **2009**, *42*, 6777–6783.
(28) Bates, S. F.; Fredrickson, G. H. *Annu. Rev. Phys. Chem.* **1990**, *41*, 525–557.
(29) Watanabe, H.; Ishida, S.; Matsumiya, Y.; Inoue, T. *Macromolecules* **2004**, *37*, 1937–1951.
(30) Watanabe, H.; Ishida, S.; Matsumiya, Y.; Inoue, T. *Macromolecules* **2004**, *37*, 6619–6631.
(31) Watanabe, H.; Matsumiya, Y.; Inoue, T. *Macromolecules* **2002**, *35*, 2339–2357.
(32) Ferry, J. D. *Viscoelastic Properties of Polymers*, 3rd ed.; Wiley: New York, 1980; Chapter 11, pp 264−320.
(33) Doxastakis, M.; Kitsiou, M.; Fytas, G.; Theodorou, D. N.; Hadjichristidis, N.; Meier, G.; Frick, B. *J. Chem. Phys.* **2000**, *112*, 8687–8694.
(34) Doxastakis, M.; Chrissopoulou, K.; Aouadi, A.; Frick, B.; Lodge, T. P.; Fytas, G. *J. Chem. Phys.* **2002**, *116*, 4707–4714.
(35) Watanabe, H.; Chen, Q.; Kawasaki, Y.; Matsumiya, Y.; Inoue, T.; Urakawa, O. *Macromolecules* **2011**, DOI: 10.1021/ma102596b.
(36) Fetters, L. J.; Lohse, D. J.; Colby, R. H. *Chain Dimensions and Entanglement Spacings*, in *Physical Properties of Polymers Handbook*, 2nd ed.; Mark, J. E., Ed.; Springer: New York, 2007; Chapter 25, pp 445−452.
(37) Watanabe, H. *Prog. Polym. Sci.* **1999**, *24*, 1253–1403.
(38) Weak and slow dielectric modes are more sensitively detected by $\Delta\varepsilon'$ than by ε'', as noted in Figure 4. This difference can be understood from the expression of $\Delta\varepsilon'$ and ε'' in terms of the dielectric spectrum $\{g_p,\tau_{p,\varepsilon}\}$,[23] $\Delta\varepsilon' = \omega^2 \Sigma_{p\geq 1} g_p \tau_{p,\varepsilon}{}^2/(1+\omega^2\tau_{p,\varepsilon}{}^2)$ and $\varepsilon'' = \omega \Sigma_{p\geq 1} g_p \tau_{p,\varepsilon}/(1+\omega^2\tau_{p,\varepsilon}{}^2)$. The $g_p\tau_{p,\varepsilon}{}^2$ factor involved in the expression of $\Delta\varepsilon'$ magnifies the weak but slow modes more significantly compared to the $g_p\tau_{p,\varepsilon}$ factor for ε''.
(39) In the PI/PtBS42 blend with w_{PI} = 55.7 wt%, the PtBS42 chain has the mass concentration, C_{PtBS} = 0.41 g cm^{-3}, and the overlapping concentration, $C_{PtBS}{}^* = \{M_{PtBS}/N_A\}/\{4\pi R_{g,PtBS}{}^3/3\}$ = 0.13 g cm^{-3}, the latter being evaluated from the root-mean-square radius of gyration reported in literature,[36] $R_{g,PtBS}/\mathrm{nm} = 0.0245 M_{PtBS}{}^{1/2}$.
(40) Rizos, A. K.; Fytas, G.; Semenov, A. N. *J. Chem. Phys.* **1995**, *102*, 6931–6940.
(41) Karatasos, K.; Anastasiadis, S. H.; Semenov, A. N.; Fytas, G.; Pitsikalis, M.; Hadjichristidis, N. *Macromolecules* **1994**, *27*, 3543–3552.
(42) Adachi, K.; Nishi, I.; Doi, H.; Kotaka, T. *Macromolecules* **1991**, *24*, 5843–5850.
(43) Yao, M. L.; Watanabe, H.; Adachi, K.; Kotaka, T. *Macromolecules* **1992**, *25*, 1699–1704.
(44) Yoshida, H.; Watanabe, H.; Adachi, K.; Kotaka, T. *Macromolecules* **1991**, *24*, 2981–2985.
(45) Watanabe, H.; Urakawa, O.; Kotaka, T. *Macromolecules* **1993**, *26*, 5073–5083.
(46) Watanabe, H.; Urakawa, O.; Kotaka, T. *Macromolecules* **1994**, *27*, 3525–3536.
(47) Fetters, L. J.; Lohse, D. J.; Richter, D.; Witten, T. A.; Zirkel, A. *Macromolecules* **1994**, *27*, 4639–4647.
(48) Fetters, L. J.; Lohse, D. J.; Graessley, W. W. *J. Polym. Sci., Part B: Polym. Phys.* **1999**, *37*, 1023–1033.
(49) Pathak, J. A.; Kumar, S. K.; Colby, R. H. *Macromolecules* **2004**, *37*, 6994–7000.
(50) (a) The Kuhn molecular weight of PtBS, $M_{K,PtBS} \cong 1500$, was evaluated from the data for the characteristic ratio ($C_\infty = 13.0 \pm 0.7$)[50b] and a ratio of the mean-square end-to-end distance to molecular weight reported for PtBS,[36] $\langle R_{PtBS}{}^2\rangle/\mathrm{nm}^2 = 3.6_1 \times 10^{-3} M_{PtBS}$. (b) Mays, J. W.; Ferry, W. M.; Hadjichristidis, N.; Funk, W. G.; Fetters, L. J. *Polymer* **1986**, *27*, 129–132.
(51) Chen, Q.; Matsumiya, Y.; Hiramoto, K.; Watanabe, H. *Polym. J.* **2011**in press.
(52) The iso-τ_s temperature T_{iso} determined from the standard WLF analysis is often referred to as the *iso-frictional* temperature in literature including our previous papers.[25,26] Strictly speaking, τ_s is proportional to $\zeta_s(T)/T$, not just to ζ_s. It is the ζ_s/T ratio, not ζ_s, that has the same value in the blend and bulk at respective T_{iso} determined from the WLF analysis of the shift factor. Nevertheless, the T dependence of ζ_s is much stronger than that of $1/T$ (with T in K unit) so that the friction coefficient ζ_s is almost the same in the blend and bulk at respective T_{iso}.
(53) Stockmayer, W. H.; Kennedy, J. W. *Macromolecules* **1975**, *8*, 351–355.
(54) The τ_ε(T) of the copolymer, defined by eq 1, were evaluated from the low-ω tails of the dielectric data that violated the time−temperature superposition. Thus, the temperature dependence of $\tau_\varepsilon(T)$

shown in Figure 7 is a little different from the dependence of the dielectric shift factor $a_{T,\varepsilon}$ shown in Figure 5, the latter being obtained from the dielectric data at high $\omega \geq \omega_{peak}$.

(55) Chen, Q.; Uno, A.; Matsumiya, Y.; Watanabe, H. *Nihon Reoroji Gakkaishi (J. Soc. Rheol. Jpn.)* **2010**, *38*, 187–193.